

UCLA

UCLA Electronic Theses and Dissertations

Title

Characterization of Transcortical Porosities During Periodontal Disease in Rats

Permalink

<https://escholarship.org/uc/item/83m802mk>

Author

Lum, Andrew G

Publication Date

2022

Peer reviewed|Thesis/dissertation

UNIVERSITY OF CALIFORNIA
Los Angeles

Characterization of Transcortical Porosities During Periodontal Disease in
Rats

A thesis submitted in partial satisfaction of the
requirements for the degree Master of Science in
Oral Biology

by

Andrew Gary Lum

2022

© Copyright by
Andrew Gary Lum
2022

ABSTRACT OF THE THESIS

Characterization of Transcortical Porosities During Periodontal Disease in Rats

by

Andrew Gary Lum

Master of Science in Oral Biology

University of California, Los Angeles, 2022

Professor Sotirios Tetradis, Chair

INTRODUCTION: Cortical bone microarchitecture exhibits a level of plasticity which adapts to changes in health status. In periodontal disease, bone loss can occur as a result of bacterial plaque induced inflammation around teeth. As we learn more about the mechanisms driving periodontal bone loss, one aspect that is not well understood are the changes in cortical bone and their role in alveolar bone remodeling. Previous studies utilizing long bones have recognized the importance of cortical bone microarchitecture in understanding disease pathogenesis, and preliminary evidence suggests similarities may exist in jaw bones as well.

OBJECTIVE: The purpose of this μ CT study is to identify and characterize transcortical canal porosities in rat jaws, and to evaluate the anatomical changes in response to experimental periodontitis.

MATERIAL AND METHODS: 14 eight-week-old, Wistar Han rats underwent ligature placement, utilizing 4-0 silk sutures ligated around the left maxillary second molars, and 28-gauge stainless-steel wire around the left mandibular first molars. Contralateral molars served as non-ligated control teeth in each animal. Animals were monitored to ensure ligature presence, and randomly assigned to euthanasia 2 or 4-weeks after ligature placement. Maxillae and mandibles were trimmed, placed in 10% formalin for 48-hours, then stored in 70% ethanol for μ CT imaging at 15 μ m and 5 μ m resolution. CTan imaging software was used to quantify vertical bone loss circumferentially at 15 μ m resolution. A global threshold was applied to segment transcortical canal spaces at 5 μ m resolution, in order to quantify number and size of canals.

RESULTS: At 15 μ m resolution, three-dimensional reconstructions of the buccal cortical bone exhibited increased porosity in the presence of ligature-induced experimental periodontitis, over healthy non-ligature molars. Further analysis of selected binarized slices at 5 μ m resolution, revealed an increase in number and volumetric percentage of intracortical porosities in experimental periodontitis molars compared to non-ligature controls.

CONCLUSIONS: Our observations demonstrate a complex network of canals exists within the cortical jaw bones of healthy rats. After 2-weeks of experimental periodontitis, an increase in the size and number of transcortical canals was observed, indicating that cortical bone morphology is highly dynamic in response to oral disease. These results enhance our current understanding of bone microstructure and disease driven adaptation. Our ongoing studies are directed at further interrogating the role of intracortical canals in oral inflammatory bone remodeling.

The thesis of Andrew Gary Lum is approved.

Jimmy Kuanghsian Hu

Mohammed Abbas Husain

Perry Klokkevold

Flavia Queiroz De Mo Pirih

Sotirios Tetradis, Committee Chair

University of California, Los Angeles

2022

ACKNOWLEDGEMENTS

I would like to thank my mentors and colleagues who have helped me throughout my academic career. From Lynbrook High School, UC San Diego and Tufts School of Dental Medicine, to my time at the National Institutes of Health and finally at UCLA, I owe a tremendous amount of my success to their guidance and preparation.

Lastly, I would like to thank my family and loved ones who have supported me with never ending patience and wisdom.

TABLE OF CONTENTS

ABSTRACT OF THE THESIS	ii
COMMITTEE	v
ACKNOWLEDGMENTS	vi
LIST OF FIGURES	ix
I. INTRODUCTION	
A. Periodontal disease and alveolar bone remodeling	1
B. Bone architecture	1
C. Transcortical canals	3
D. Hypothesis and aims	6
II. MATERIALS AND METHODS	
A. Animals	7
B. Ligature placement	7
C. Ex-vivo MicroCT (μ CT) scanning	8
D. Statistical Analysis	9
IV. RESULTS	
A. Clinical assessment	11
B. Linear bone loss in maxilla	11
C. Volumetric changes to transcortical pores in maxilla	12
D. Linear bone loss in mandible	14
E. Volumetric changes to mandibular buccal plate	14
F. Changes in transcortical porosities in mandible	15
V. DISCUSSION	16

VI.	CONCLUSIONS	30
VII.	FIGURES	31
VIII.	REFERENCES	50

LIST OF FIGURES

Figure 1	Rat weight at start and end of each experimental period	31
Figure 2	Clinical assessment of soft tissues	31
Figure 3	Circumferential bone loss around maxillary molars	33
Figure 4	Buccal plate bone loss around maxillary molars	34
Figure 5	Analysis of maxillary bone volume and porosity	35
Figure 6	Proportion of maxillary buccal bone and porosity	36
Figure 7	Number of maxillary buccal plate pores	37
Figure 8	Average volume of maxillary buccal plate pores	39
Figure 9	Circumferential bone loss around mandibular molars	40
Figure 10	Buccal plate bone loss around mandibular molars	42
Figure 11	Analysis of mandibular bone volume and porosity	44
Figure 12	Proportion of mandibular buccal bone and porosity	45
Figure 13	Number of mandibular buccal plate pores	47
Figure 14	Average volume of mandibular buccal plate pores	49

INTRODUCTION

Periodontal disease and alveolar bone remodeling:

Periodontal disease affects approximately half of the adult US population, and the consequences of untreated disease can involve irreversible bone loss and early tooth loss (Eke et al., 2015). Under healthy conditions, our oral immune system remains quiescent in response to low levels of oral microbiota and thus the natural bone remodeling process remains homeostatic. However, if the oral biofilm shifts towards dysbiosis, an aberrant host inflammatory response can lead to changes in the gingival soft tissue, and drive alveolar bone remodeling in the direction of resorption (Hajishengallis, 2015). Severe bone loss typically occurs at the bone crest, adjacent to biofilm accumulation and the inflammatory nidus, and can increase susceptibility for early tooth loss. In addition, uncontrolled periodontal disease can have negative effects on overall health and compound systemic diseases such as diabetes (Taylor et al., 2013). As a result, one of the common noninvasive methods for determining the rate and severity of periodontal disease relies on visualizing interproximal bone loss using two-dimensional radiographs (Armitage, 1996).

Bone architecture:

Bone is a rigid organ that provides support and structure for many vertebrate animals, and is composed of a mineralized connective tissue

matrix. Bone macrostructure can be divided into outer cortical and inner cancellous layers which vary in arrangement and density depending on the mechanical or biological demands of that area. Cortical bone consists of successive arrangements of collagen matrix that are first organized into sheets called lamellae, and then into larger cylindrical structures known as osteons (Weiner et al., 1999; Zimmermann et al., 2011). Osteons collectively make up the Haversian system which runs parallel to the long axis of the bone. First described in humans by Clopton Havers in 1691, Haversian canals contain neurovascular bundles, osteocytes, and are oriented to maintain structural integrity of dense cortical bone. In the 18th century, Alfred Volkmann observed canals that run obliquely to Haversian canals, providing anastomosis and connections between the periosteum which lays external to bone and the endosteum which lines the innermost aspect of bone. The organization of cortical bone into Haversian and Volkmann's networks, contrasts with trabecular bone which forms a porous inner network of bones and consists of a sparsely distributed lamellar network. The sinuous nature of trabecular bone is necessary for maintaining structural integrity while also allowing space for the medullary cavity which facilitates cell and nutrient transportation and houses the bone marrow (Enlow, 1962; Oftadeh et al., 2015).

The cellular composition of bone includes four primary types of cells, making bone uniquely vital: Osteoclasts, osteoprogenitor cells, osteoblasts, and osteocytes. Osteoclast help regulate bone mass by orchestrating resorption which can occur on trabecular surfaces for modulation of mineral homeostasis, as well as on cortical surfaces to promote neovascularization (Clarke, 2008; Lafage-Proust et al., 2015). Osteoprogenitor cells reside primarily within the bone marrow and the periosteum, and are prepared to give rise to osteoblasts and osteocytes. Osteoblasts contribute to new bone formation and skeletal maintenance by secreting organic and inorganic matrix proteins that coordinate matrix mineralization (Blair et al., 2017; Yee et al., 2019). Once osteoblasts are surrounded by bone, they mature to become osteocytes, representing a highly numerous and organized network for communicating with other osteoblasts, and providing hormonal signals to the systemic circulation (J.-M. Kim et al., 2020; Metzger & Narayanan, 2019; O'Brien et al., 2008; Yan et al., 2020)

Transcortical Canals:

Recent studies on cortical bone microstructure in small animals have shown a complex network of intracortical canals in existence that exhibit resemblance to previously described Haversian System and Volkmann's Canals in humans. Indeed, cortical bone which makes up to 80% of the skeletal mass is not only structural but vital and functional. These

intracortical canals are believed to provide osteocytes with access to nutrients within the bone marrow, and the opportunity to communicate with distant organs that regulate overall bone and mineral health (Intemann et al., 2020; Root et al., 2020). Furthermore, while the dense cortical bone may provide rigidity and structural integrity, it also poses challenges for rapid access to the endosteum. Transcortical canals facilitate neurovascular and nutrient networks to the periosteum, and serve as a key mechanism for osteocyte bone remodeling in response to inflammation (Grüneboom et al., 2019). This study identified transcortical vessels in the size range of 10-11 μ m that traversed cortical bones of mouse femurs, and expressed endothelial and immune cell markers, thus contributing to immune cell transport between the periosteum and bone marrow. Importantly, medication and disease induced states led to mobilization of neutrophils, osteoclastic remodeling of canals, as well as new canal formation, implicating the powerful role these canals play in mediating overall bone physiology.

Many studies of transcortical canals have looked at murine long bones, utilizing μ CT imaging to demonstrate the complex vascular network that exists within dense cortical bone. This approach overcomes the challenges of traditional imaging techniques that may be destructive to the specimen or misrepresent the three-dimensional nature of bone (D. M. L. Cooper et al.,

2003; Núñez et al., 2017; Tanaka et al., 2011). MicroCT imaging in the scale of 5-10 μ m resolution has become an accessible tool for enhancing documentation of small-scale morphologic differences that were not attainable in the past, and thus introduced new and exciting information for investigating the mechanical and biologic properties of bone. Interestingly, microscopic observations suggest that transcortical canals are not limited to long bones, but do in fact exist within the alveolar buccal bone of humans, and may have a similar relationship by connecting the soft tissue and periosteum with the underlying trabecular bone network during health and disease (Iezzi et al., 2020).

In clinical practice, elevating a full-thickness mucoperiosteal flap will sever an in-tact periosteum, and any potential vascular connections to the cortical bone; this can lead to unwanted gingival recession or loss of the alveolar bone width due to a compromised blood supply (McLean et al., 1995). In the presence of disease and inflammation, radiographic studies of have shown evidence of collapsed canals within cortical bone (J.-N. Kim et al., 2015; Y. Kim et al., 2018). However, μ CT studies have yet to fully characterize the microstructural changes that occur within alveolar cortical bone to the level that has been seen with long bones. Utilizing high-resolution μ CT imaging to characterize the microstructural changes in rodent alveolar cortical bone during health and disease represents a valuable asset to enhance our

understanding of the fundamental dynamics of bone biology, and disease management.

Hypothesis and Aims:

As a result, we hypothesize that an organized network of canals exists within the cortical bone of rat jaws. These canals vary in size and quantity during periodontal disease, and this plasticity may contribute to the pathologic changes seen during bone remodeling. To test this hypothesis, the ligature induced periodontitis rat model provides well-documented clinical simulation of adult chronic periodontitis. To further elucidate the role of transcortical canals, we propose the following aims: Identify and characterize transcortical canals in rats using μ CT scanning, and to evaluate anatomic changes in transcortical canals of rat jaw bones during periodontal disease.

MATERIALS AND METHODS

Animals:

14 eight-week-old, healthy, male Wistar Han rats (Charles River Laboratories, Raleigh, NC) were treated according to the guidelines and protocols of the Chancellor's Animal Research Committee of the University of California, Los Angeles. Throughout the duration of the experiment, rats were housed (2 rats per cage) in pathogen-free conditions with a 12-hour light/dark cycle, and fed a standard laboratory diet (NIH-31 Modified Open Formula, ENVIGO, Madison, WI), and given water ad-libitum.

Ligature placement:

Rats were anesthetized using isoflurane and ligatures were placed around the cervical region of left maxillary and mandibular molars. 4-0 silk sutures were used to ligate the left maxillary second molar, and 28-gauge stainless-wire was used around the left mandibular first molar. Contralateral molars served as non-ligated control teeth in each animal. Rats were monitored every three days to measure weight and ensure ligature presence, and replacement if missing. Each animal was randomly assigned at the beginning of the experiment to be euthanized after 2 or 4-weeks of ligature placement. Maxillae and mandibles were trimmed, and clinical images were immediately taken using a digital microscope, then specimens were placed in 10% formalin for 48-hours, before being stored in 70% ethanol at 100°C.

Ex-vivo MicroCT (μ CT) scanning:

Dissected maxillae were imaged by high-resolution ex vivo μ CT utilizing the SkyScan 1172 μ CT scanner (SkyScan, Kontich, Belgium) at 15 μ m and 5 μ m resolution utilizing 55kVP and 181 μ A. Both linear and volumetric measurements were collected to assess periodontal bone loss and changes to cortical bone microarchitecture. Image data were reconstructed into three-dimensional volumes with NRecon software (Version 1.7.0.4, Bruker). Linear bone loss was measured at 15 μ m resolution as the distance from the cemento-enamel junction (CEJ) to the alveolar bone crest (ABC). This measurement was repeated circumferentially around each tooth at 3 positions along the buccal, palatal or lingual plates, and interproximal, then averaged to a mean linear bone height.

Volumetric analysis of the cortical bone porosity was performed on the buccal plate of maxillary and mandibular molars utilizing the 5 μ m resolution scans. All teeth were rotated until the occlusal table was parallel to the horizontal plane in a mesial-distal direction, and a buccal-lingual or buccal-palatal direction. First a volume of interest was established by defining a region limited to the buccal bone directly adjacent to the tooth root of interest, using the frontal slices of the appropriate jaw. On mandibular 1st molars, the mesial-buccal, mid-buccal, and distal-buccal roots each included

100, 40, and 60 trans-axial slices, respectively. On maxillary 2nd molars, the mesial-buccal and distal-buccal roots included 40, and 60 slices, respectively. After the mesial and distal extent of the buccal cortical bone were defined, the lateral borders were defined by the margin of bone facing periosteum and the periodontal ligament space. The region of interest extended to the crestal border of alveolar bone, and the apical extent of the tooth.

Identification, quantification, and 3D reconstruction of the buccal cortical plate porosities was performed through a custom processing batch in CTAn. First, a global threshold was applied (70-255) and despeckled to generate a model of the entire cortical plate. From this volume, subtractive despeckling of open or closed pores and inversion generated 3D models and individual object analysis of transcortical porosities within the designated buccal plate region. Individual and overall characteristics were recorded: individual number and size of transcortical spaces, as well as overall bone porosity representing pattern changes in transcortical canals.

Statistical Analysis:

Linear bone height, volumetric analyses, and transcortical porosity quantification were represented as mean \pm standard error of the mean. A

paired t-test for means was used to compare significance between ligature and non-ligature groups with a significance level set at <0.05 .

RESULTS

Clinical assessment:

The average initial body weight of all 14 rats was $310.4\text{g}\pm 7.5$ (mean \pm SD). The average body weight for all rats at the conclusion of the 2-week and 4-week experimental time points were $319.0\text{g}\pm 11.0$, and $299.0\text{g}\pm 8.2$, respectively (Figure 1). A statistically significant increase in body weight was observed between the initial and 2-week timepoints. However, no changes in weight were observed when comparing the initial vs. 4-week timepoints.

Wire and silk ligature presence was confirmed every third day during the experiment, and if missing or loose, was replaced with the appropriate material. Clinical microphotographs did not show any noticeable differences in soft tissue texture, tone, or consistency, but close adaptation of the ligature, as well as debris accumulation was evident compared to the contralateral control tooth (Figure 2). There were no observable clinical differences in the periodontium between the 2-week vs. 4-week groups.

Linear bone loss in maxilla:

In order to verify the capacity for silk ligature to induce periodontal bone loss, the maxillae were scanned utilizing μ CT at $15\mu\text{m}$ resolution and analyzed for linear bone height differences between CEJ and ABC at 3 separate positions along the buccal bone, palatal bone, and interproximal to

the mesial and distal of each tooth. The root of the molar tooth, or the furcation entrances were used as consistent landmarks for measurements.

Placement of a silk ligature induced significant increase of the CEJ-ABC distance at 2-weeks, and 4-weeks. In addition, while the furcation bone remained stable throughout control teeth, radiographic signs of furcation bone loss were evident in all ligated teeth (Figure 3A, B, C). Upon inspection of the changes occurring to the buccal plate alone, there was also a significant increase in the CEJ-ABC distance between the 2-week vs. 4-week groups (Figure 4).

Interestingly, multiplanar assessment of the alveolar ridge demonstrated periosteal bone formation in the ligature site at both the 2-week and 4-week timepoints (Figure 5A). Thus, we elected to assess volumetric changes of the alveolar ridge, in addition to the changes in bone height. Investigation into the volumetric changes of the buccal cortical plate revealed that ligature placement induced an overall increase in the total buccal plate volume. Quantification of the buccal plate showed that the difference was initially evident at the 2-week timepoint, and became statistically significant at the 4-week timepoint compared to the non-ligature control group (Figure 5B).

Volumetric changes to transcortical pores in the maxilla:

Application of the global threshold segmented radiopaque areas of bone from radiolucent areas of intracortical porosity. At 2-weeks, ligature placement resulted in a significant decrease in bone volume compared to the baseline control. At 4-weeks, the ligated molars showed a significant increase in bone volume compared to the 4-week control sites (Figure 5C).

The total volume of transcortical porosities in the maxillary buccal plate were determined from the same global threshold which segmented radiolucent and radiopaque areas corresponding to visible pores traversing within the cortical bone. There was a statistically significant increase in the total volume of transcortical porosities after ligatures were in place for the 2-week or 4-week groups (Figure 5D). The overall make-up of the buccal cortical plate at all timepoints was 81% bone, and 19% porosity (Figure 6). At 2 and 4-weeks, there was a similar percentage of both cortical bone and porosity in healthy sites, whereas ligature placement at 2-weeks resulted in a higher percent porosity compared to the ligature placement after 4-weeks, 23% vs. 12%, respectively.

After segmentation of individual open and closed pores, there was an overall increase in the number of pores within the maxillary buccal plate after ligature placement. However, while there was a slight increase at 2-weeks, the number of pores did not significantly increase until the 4-week timepoint

(Figure 7). In order to better understand dynamic changes in the transcortical canals, individual changes to the pore volume were analyzed. There was a significant increase in pore volume in the ligature vs. healthy site of the 2-week group. At 4 weeks, no differences in the pore volume between the healthy vs. ligature sites were detected (Figure 8).

Interestingly, there was a noticeable decrease in the average size of pores in the ligature site of 4-week vs. 2-week groups. Compared to their respective control teeth, ligature placement resulted in an overall increase in the average individual pore volume.

Linear bone loss in mandible:

MicroCT analysis of healthy, non-ligature mandibular teeth revealed normal alveolar bone architecture, without any signs of buccal plate expansion across the 4-week experimental period. In addition, the distance from CEJ-ABC of all control teeth were consistent through 4-weeks, without significant changes compared to baseline. The ligated site of mandibular molars showed a statistically significant increase in vertical bone loss, when compared with the non-ligated control sites (Figure 9). A similar pattern of bone loss was found at the interproximal bone and lingual bone, although mild periosteal bone reaction was only apparent along the buccal plate (Figure 10).

Volumetric changes to mandibular buccal plate:

Volumetric changes to the mandibular buccal plate followed a general trend which was similar to that observed in the maxillary buccal plate. However, quantitatively and qualitatively, increased porosity and periosteal bone formation of the mandibular buccal plate was not as substantial as in the maxillary buccal plate. Significant differences between the ligature vs. healthy sites were seen only for increased porosity and increased % porosity in the 2-week group. When 2-week and 4-week groups were combined, an overall significant difference between the ligature vs. healthy sites was noted for total buccal plate volume, porosity volume, and % porosity (Figure 11, 12).

Changes in transcortical porosities in mandible:

A uniform pattern of increasing buccal plate porosity was seen at the ligature sites. However, these differences did not reach significance for neither the 2-week nor the 4-week timepoints. When the two timepoints were combined, a significant increase in the number but not in the volume of pores was seen (Figure 13, 14).

DISCUSSION

Periodontal disease remains a major health burden for many adults in the United States. Unmanaged, this chronic disease can result in severe loss of a tooth's supporting structures and the irreversible damage can become an obstacle for tooth maintenance, retention, and oral rehabilitation. Although our oral cavity normally tolerates a low level of inflammation, disturbances in the form of microbial dysbiosis and biofilm accumulation can initiate an aberrant inflammatory response by the host (Pihlstrom et al., 2005). As a result, pro-inflammatory factors and stimulators of bone resorption drive osteoclast activation and resorption of the bone around teeth. In addition, circulation of proinflammatory mediators responsible for periodontal breakdown have been linked to diabetes, thus stressing the importance of properly diagnosing, managing, and treating periodontal disease for overall patient health (SILVA et al., 2015).

Throughout the day bacterial plaque accumulates on teeth at the dentogingival complex and adjacent to this site is the alveolar crest, where bone loss during periodontitis begins. Over time, bone loss will progress in an apical direction until the tooth is lost and the inflammatory burden has been removed. Routine mechanical removal and disturbance of the subgingival biofilm remains the gold standard for prevention and treatment of periodontal bone loss, as there is limited evidence supporting

chemotherapeutics or laser therapy (Pawelczyk-Madalińska et al., 2021). Progression of periodontal disease varies significantly among patients. However, the mechanisms responsible for periodontal inflammation and resultant alveolar bone remodeling remain largely unclear, thus hindering our ability to accurately predict or prevent conditions which make certain patients more susceptible. For example, elevating a mucoperiosteal flap is often unavoidable, but in the presence of thin cortical bone results in excessive bone remodeling (Chappuis et al., 2017).

Much of the research in periodontal disease has focused on the bacterial biofilm biology or the host inflammatory response mounted in the gingival tissues. Periodontal bone loss often is studied as the ultimate phenotypic indication of tooth support and disease burden. Yet, the mechanisms that mediate periodontal bone loss and affect homeostasis have not been delineated. Understanding alveolar bone remodeling will not only provide important insights in periodontal disease onset and progression, but will also inform pathophysiology of other diseases that affect the alveolar bone, such as osteoradionecrosis (ORN), medication related osteonecrosis of the jaws (MRONJ), osteomyelitis or response of the alveolar bone to systemic metabolic disorders or metastatic malignancy.

Bone remodeling occurs via the coordinated interaction of bone forming osteoblasts and bone resorbing osteoclasts in a well-recognized organized structure called basic multicellular unit (BMU). In the cortical bone, the osteoclasts “cutting” and osteoblasts “closing” of bone, result in secondary osteon formation within the Haversian system. As osteoblasts mature, they become embedded in cortical bone and transform into osteocytes, a cell with extensive dendritic process that has a central role in regulating further bone remodeling (Bonewald, 2011).

Early studies have shown distinct changes in cortical bone microarchitecture in the presence of periodontal disease (Kishi et al., 1982). Utilizing high resolution contact x-rays to visualize alveolar bone affected by periodontal disease detailed the presence of vascular channels and perforations forming an anastomosing network between the external cortical bone and cancellous trabecular space (Moskow et al., 1985). Recent contributions to the literature have outlined mechanisms for cortical bone anatomy and remodeling in other skeletal sites. However, little is known about the cortical bone changes during periodontal disease. As a result, the goal of this study was to identify transcortical canals in rodents and characterize the anatomic changes that occur between health and periodontal disease.

When cortical bone microstructure in humans was initially described in 1691 by Clopton Havers, the Haversian system represented longitudinal channels surrounding neurovascular bundles and was believed to support medullary transport along the length of cortical bone. Transverse canals providing additional connection to the outer periosteum were later renamed Volkmann's canals, but our general view on cortical bone pathways has largely remained the same. However, evidence from histology and microscopy studies have suggested that there is more complexity to these structures than the original description suggests (Ascenzi, 2012). Three-dimensional imaging and reconstruction of human femurs displayed this complexity in the form of anastomosing vascular networks, species specificity, and adaptive changes in resorptive patterns (D. M. L. Cooper et al., 2003, 2004). Scanning electron microscopy also suggests the well referenced Haversian system represents only a portion of a more complex lamellar architecture in rabbit long bones. Canal diameter in this study ranged from 30-1000 μ m and canal openings condensed along the endosteal surface. Combined with existing studies on blood flow dynamics, it appears that these canals created by osteoclasts originate from the marrow network rather than the periosteal surface (Pazzaglia et al., 2009).

In our experiments, we were able to show existence of transcortical porosities, arranged in canal-like spaces within the buccal alveolar bone, in

the absence of any disease. These spaces penetrated the entire cortical bone depth, and were present throughout the buccal plate in both maxillary and mandibular jaws of healthy, male rats aged 16-18 weeks.

Recently, the use of synchrotron μ CT and higher resolution imaging have made it possible to image these intracortical canals and their soft tissue constituents with greater detail and minimal bias compared to traditional microscopy or histologic approaches (BRITZ et al., 2010; D. M. L. Cooper et al., 2011). In another comparative μ CT study analyzing human cortical bone porosities, intracortical canals were shown using 5–15 μ m resolution, but increasing voxel size resulted in deterioration of the clarity, and thus affected qualitative parameters such as cortical porosity, canal number, canal size, and density of canals (D. Cooper et al., 2007).

Due to improvements in μ CT imaging quality, studies have identified cortical bone porosities ranging from 0.7-7 μ m, but variations have also been reported depending on species, anatomic location, and health status. In addition, the field of view size, resolution and thresholding technique influence porosity size (Martín-Badosa et al., 2003; Schneider et al., 2007; Sietsema, 1995). Another study aimed at optimizing scan resolutions between 1-5 μ m found that canal diameter measured 22 μ m when utilizing 1 μ m scanning resolution, and significantly less at 4 μ m resolution (15 μ m

diameter). From this same study, average cortical porosity was 5% at 1 μ m resolution, and 2% using 4 μ m resolution, therefore suggesting resolution is a major source of variation in measured parameters and higher resolution may be effective for assessing cortical bone microarchitecture (Palacio-Mancheno et al., 2014). Based on these previous findings, we utilized 5-15 μ m as our scan resolution, and our observed 4% cortical bone porosity in healthy rats was within range of previously reported studies. In addition, this range was selected for its short scan time, and large field of view, which allowed us to simultaneously assess macro-scale changes circumferentially around the ligated tooth. While our findings revealed differences in cortical porosity between the maxilla and mandible, this may be partly due to inherent challenges in reconstructing complete canals at 5 μ m resolution. Particularly in the mandible, the number of pores reported was significantly higher than expected despite the decreased vascularity commonly seen. We attribute this observation to the poor contrast between the canal and the highly dense mandibular bone, which resulted in single canals appearing fragmented. If we were to assume the mandible did remodel but to a lesser degree compared to the maxilla, an increased susceptibility for diseases with a vascular component would be expected in the mandible. Nevertheless, based on preliminary observations of healthy rats at 1 μ m resolution, we strongly believe these fragmented porosities in the mandible do in-fact

represent complete transcortical canals and further studies are underway to confirm their continuity with corresponding histology.

To the best of our knowledge, our study is one of the first to investigate patterns in transcortical porosity as a result of ligature induced periodontitis. Bone loss was induced in a vertical direction circumferentially around ligated teeth, as expected. However, localized changes to the buccal bone thickness necessitated further investigation of the buccal cortical bone. When evaluating the cortical porosities of the buccal plate, an increase in the number and volume of porosities occurred at ligated sites along with an increase in the overall buccal plate volume after just 2-weeks. At 4-weeks, the number of porosities continued to increase, but surprisingly a decrease in the average pore volume was observed. The decrease in the overall percentage of porosities, from 23% to 12% suggests two concurrent processes occurred: osteoclast formation of new porosities, and osteoblast formation of new compensatory bone. Further investigation at the cellular level is required to provide insights into the detailed mechanisms underlying these findings.

Average cortical bone porosity in our study ranged around 7-23% in rats with periodontal disease, and 4% in healthy rats. These deviate from the percentages reported in previous literature which has suggested 10-30%

(Jast & Jasiuk, 2013), but likely is attributed to variation in scanning technique and origin of bone, as other studies studied long bones. In 2014, Jast et al. reported canal number increased and mean canal volume and diameter decreased with age from the third to the twelfth week of age in rat tibiae, in agreement with our findings. Reported mean canal diameter ranged from 18-29 μm , and average canal volume ranged from 339 to 742 μm^3 . Canal density location was also found to be generally heterogenous, with lower canal density in the medial region of tibiae. In addition, as longitudinal growth ceased, canal orientation changed and became more branched and radially directed to continue transporting blood and nutrients between the endosteal and periosteal regions. In accordance with our findings, this suggests cortical bone morphology is dynamic, seeking to maintain vascularization, blood perfusion, and delivery of oxygen, minerals and nutrients necessary for bone vitality in health and disease.

Bone remodeling is highly adaptive and one potential explanation for the variation seen in our study is the fact that many prior studies examined human or rodent long bones, rather than jaw bones. Jawbone remodels faster than other skeletal bones, and marrow contains greater osteogenic potential (Aghaloo et al., 2010). Jaw bones in particular undergo intramembranous instead of endochondral ossification and also receive greater loading from mastication (Berendsen & Olsen, 2015). Together,

these unique attributes combined with selective time points at 2-weeks and 4-weeks may have captured different amounts of cellular activity leading to variable porosity. In addition to location and age, gender, hormone levels and physical activity have all been shown to influence angiogenesis and overall bone remodeling and might account for some of the observed differences (Eriksen, 2010; Hendriks & Ramasamy, 2020; Kusumbe et al., 2014).

Several studies have shown changes in osteocytic lacunae size and cortical porosity distribution as a result of mechanical load (Iezzi et al., 2020).

Normal loading of these bones resulted in canals that were more longitudinally oriented than immobilized tibiae (BRITZ et al., 2010).

Distribution of cortical porosities and the general orientation of Haversian canals also can reflect mechanical stress of the surrounding environment (Heřt et al., 1994; Petrtýl et al., 1996). In-turn, the specific distribution of intracortical canals and extent of canal branching affects the mechanical

force tolerance and risk of fracture in mice femurs (Schneider et al., 2013).

Evidence for hormonal regulation of osteocyte driven bone remodeling has also been reported (Qing et al., 2012). While we did not observe any specific clustering of porosities, there was increased porosity along the periosteal surface of the buccal plate at just 2-weeks that could have been a result from chronic inflammation, or mechanical loading. Initially, this bony

reaction contributed to the overall increase in total tissue volume.

Interestingly at 4-weeks, the same area became ossified and continuous with the surrounding underlying alveolar bone. This only occurred in the ligature induced periodontitis model, and suggests the induction of initial pore formation and subsequent repair may be a crucial step in the inflammatory process that also takes place in the gingival soft tissues.

Ever since observations of ground bone sections from Rodolfo Amprino in 1947 the association between age and osteon population density or intracortical porosity, due to the accumulation of osteoporotic remodeling events has been well documented (D. M. L. Cooper et al., 2006). Our results appear to support this notion of bone adaptation since we identified intracortical porosities in both existing bone but also within newly remodeled bone during periodontal disease. In addition, canal distribution on the periosteal surface has been shown to reflect extracortical blood circulation, becoming localized around areas of rapid growth. In non-haversian rodents, the cortical lamellar complexity in femurs also favors the bony periphery, creating regions of interconnectedness in the endosteal region, and the periosteal region with additional interstitial lamellae (J.-N. Kim et al., 2015).

Further investigations on transcortical pathways and their unique role in facilitating bone remodeling reported osteoprogenitor cell habitants within

the transcortical vessels of mice, as a source of osteoblasts remodeling, while osteoclasts were also identified to take part in transcortical pore formation. Despite lacking the true Haversian systems of larger organisms, transcortical vessels have the capacity to drastically remodel bone by facilitating nerve passage and cellular signaling to osteocytes within cortical bone or distant organs (Root et al., 2020; Torreggiani et al., 2013).

Interestingly, in our experiments the number of pores increased and the average volume of pores decreased in 2-weeks vs. 4-weeks of ligature induced periodontitis. This suggests an expansion of the transcortical pore network in response to inflammation, and a potential host reaction to mitigate pore expansion and diminish osteoclast activity within canals in order to avoid detriments to the overall bone integrity.

Scanning electron microscopy studies have identified osteocytic lacunae openings to the collagen lined transcortical canals, with holes ranging from 0.1-0.5 μ m in diameter believed to be channels for canaliculi originating from the osteocytic lacunae. It was reported that size and shape of the canals appear to be determined by the extent of osteoclast digging, amount of lamellar deposition by osteoblasts, and also blood flow dynamics (Metz et al., 2003; Pazzaglia et al., 2009). While our samples were not scanned at the resolution capable of detecting osteocytic lacunae, based on prior human cone beam computed tomography observations, we believe the increase in

transcortical porosity is a consequence of neovascularization induced by chronic periodontitis, supporting the idea that alveolar remodeling does not occur solely at the crestal surface, but it also occurs from within transcortical porosities. This results in decreased cortical bone density, and improved vascular and immune responsiveness to soft tissue inflammation. Evidence of vascular remnants have been shown using high resolution synchrotron x-ray phase-contrast enhanced tomography (Carulli et al., 2013; Núñez et al., 2017). Histology validated the presence of intracortical capillaries and osteocyte lacunae in conjunction with cortical bone porosities of 15-week-old mice scanned at 1.3 μ m, confirming previous studies that angiogenesis and osteogenesis are closely intertwined (Marenzana & Arnett, 2013; Schipani et al., 2009).

The presence of transcortical canal inhabitants provides functional relevance. While our findings are primarily observational, they offer important context in the realm of oral disease pathogenesis and alveolar bone remodeling. They also support the idea that cortical bone vitality is maintained by a network of transcortical canals that is more expansive and complex than the Haversian and Volkmann system. In the context of periodontal surgery, elevating a full thickness flap can easily disrupt the vascularity that supplies the underlying cortical bone. Many studies have suggested the importance of respecting this vascularity in order to maintain integrity of the thin buccal

alveolar bone (Grassi et al., 2019), but our study provides observational support of that thesis.

Recently, transcortical vessels in murine long bones were identified and shown to provide an effective pathway between the bone marrow endosteum, and external periosteum in order to maintain vascularity, circulation of nutrients and signaling molecules, and to facilitate immune cell transport (Grüneboom et al., 2019). Osteoclasts were identified in the middle of existing transcortical vessels, in contact with osteocyte canaliculi, and the presence of similar type vessels was also confirmed in human limb bones.

In our study, the presence of chronic inflammation such as periodontitis induced significant changes to the cortical bone pattern, suggesting activation of osteoclast remodeling occurs within the canals, in addition to the crestal surface of bone. Similarly, under experimental conditions of chronic arthritis, increased numbers of transcortical vessels were observed (Grüneboom et al., 2019). Mobilization of neutrophils and neovascularization was present and transcortical vessels were responsible for 80% of arterial flow. In addition, as a function of age, decreased number of transcortical vessels were observed while the overall shape remained consistent – suggesting these vessels adapt to biologic and physiologic changes, and as

osteocyte numbers decline with age, susceptibility to age-related bone injuries increase. Furthermore, transcortical vessels appear responsive to the osteoclast inhibitory effects of Zolendronate, resulting in limited transcortical vessel formation and overall poorer bone vascularization.

MicroCT provides valuable insight on the patterns and changes that occur as a result of cortical bone remodeling in rat jaws. To the best of our knowledge, this is one of the few studies to evaluate changes in cortical bone microarchitecture using a ligature-induced periodontitis rat model. Previous studies of similar nature have utilized larger mammals or long bones, and often associate transcortical canals with the Haversian System and Volkmann's canals (Asghar et al., 2020; Werner et al., 2017). However, bone formation and remodeling in larger animals or long bones does not entirely resemble that of non-Haversian rodent jaw bones. As a result, we observed that ligature induced periodontitis exhibits the greatest change in cortical bone microarchitecture along the buccal plate of maxillary molars. Upon closer assessment, we identified the presence of transcortical porosities in healthy buccal bone. Around diseased sites, there was an initial increase in new transcortical porosities, evidenced by the increase in number and volume. However, as the chronic lesion progressed, the changes were marked by a subsequent decrease in average pore volume, resulting in a

complex transcortical network that suggests immense plasticity by the host to maintain alveolar bone remodeling.

CONCLUSIONS

In conclusion, the cortical plate is a commonly overlooked parameter in the diagnosis of periodontal disease compared to the interproximal cancellous bone. However, our results demonstrate the capacity of the buccal cortical bone to remodel during periodontal disease. Thus, we believe our findings necessitate further research exploring the evolution of transcortical canals at higher resolution and correlating this with histologic findings. Ongoing studies can help elucidate their possible role in disease pathogenesis and identify potential therapeutic targets in the bone remodeling process.

FIGURES

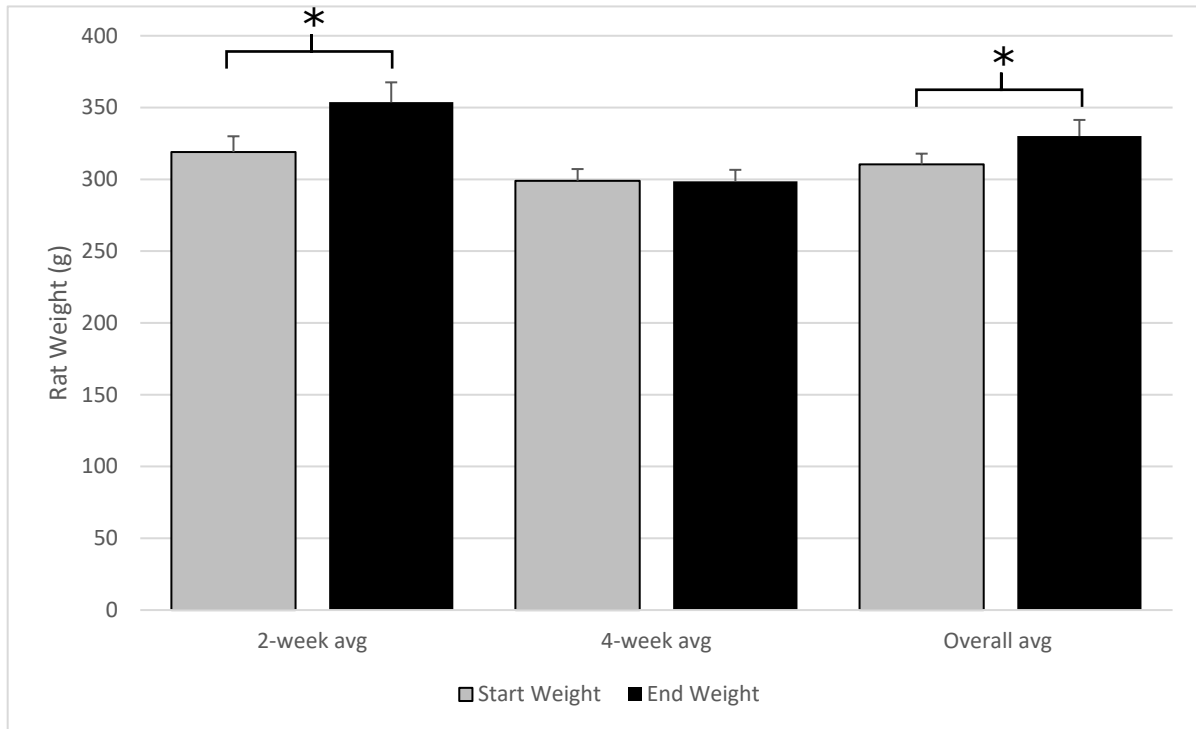


Figure 1: Rat weight at start and end of each experimental period. Data are represented as a mean \pm standard error of the mean. * $p < 0.05$, ($n \geq 6$ for all groups).

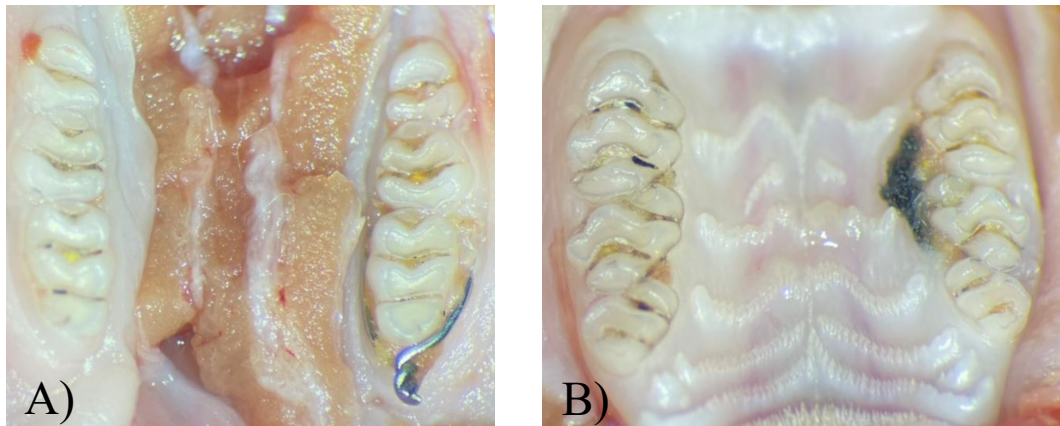


Figure 2: Clinical assessment of soft tissues. **A)** mandible, **B)** maxilla and their corresponding control (no ligature), 28-gauge stainless wire ligature, or 4-0 silk suture ligature.

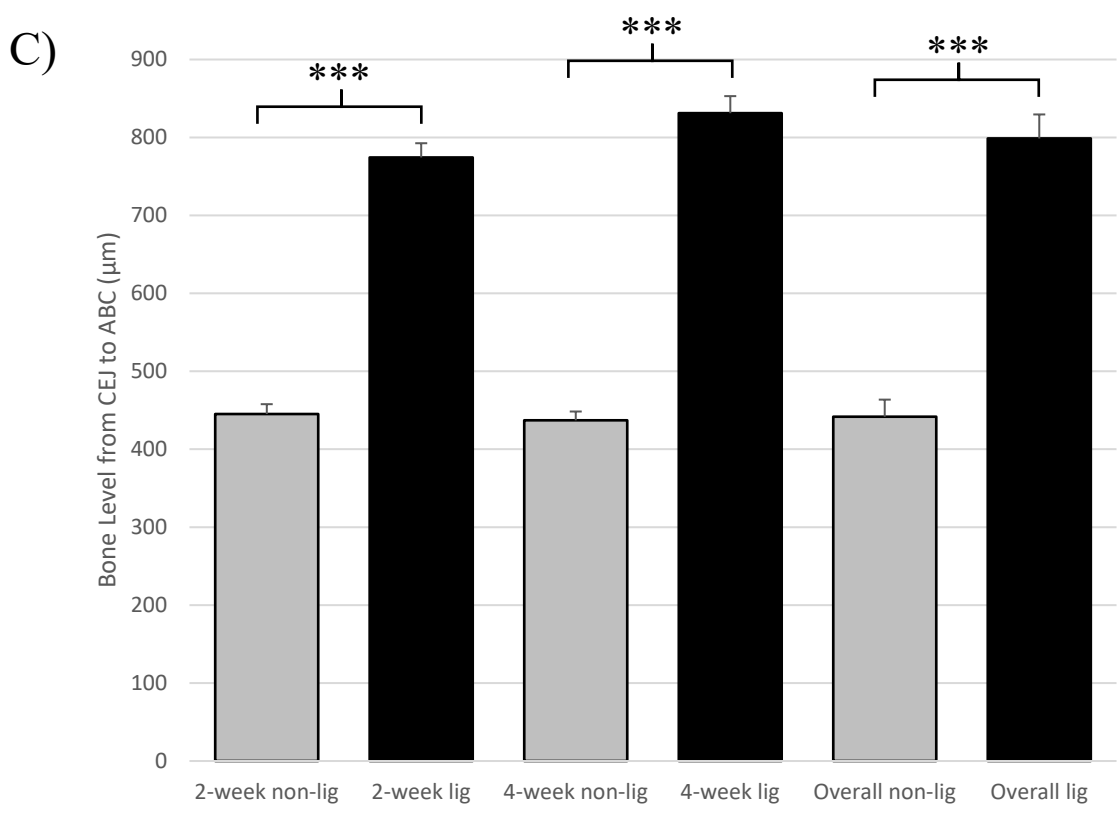
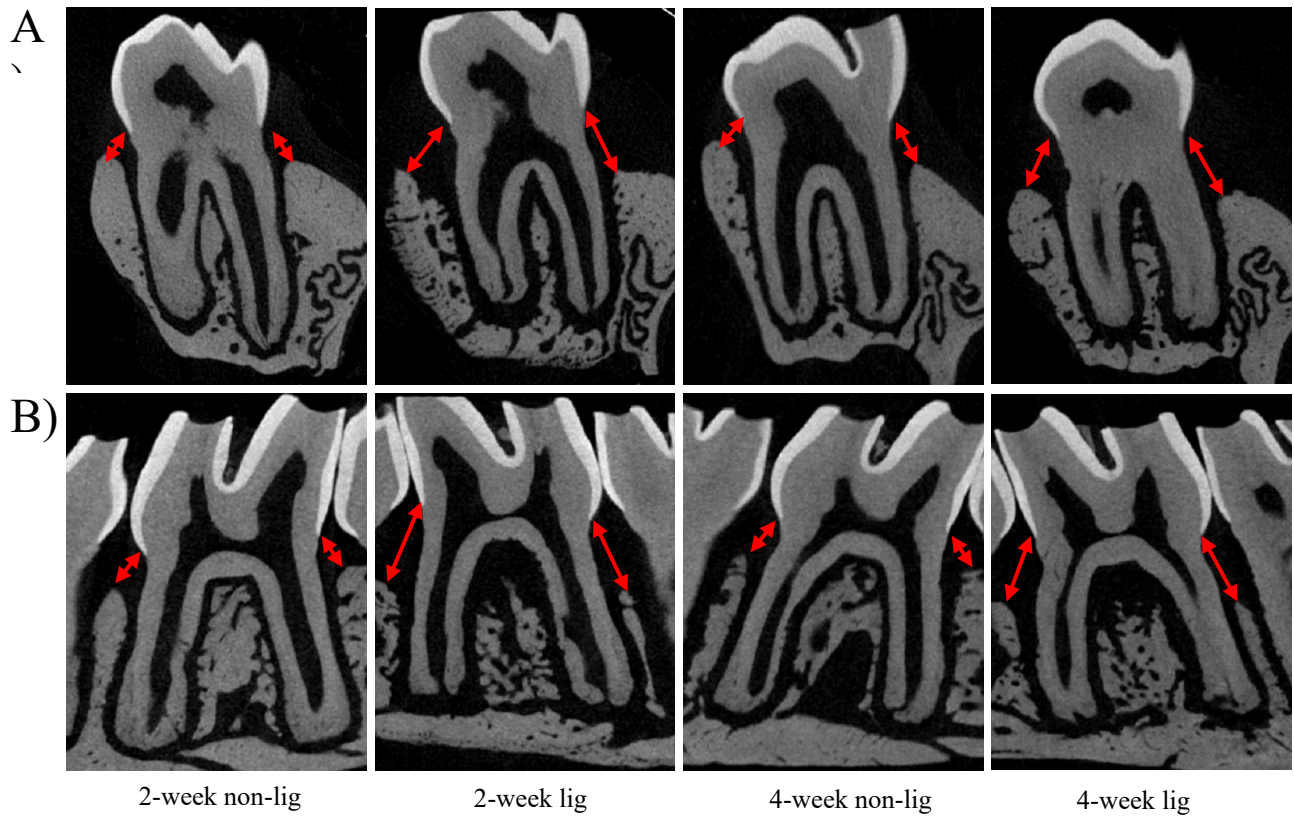


Figure 3: Representative analysis of bone loss measured circumferentially around maxillary molars **A)** Representative images of buccal and palatal bone height analysis in a sagittal plane. **B)** Representative images of interproximal bone height in a transverse plane. **C)** Comparison of non-ligature and ligature sites at 2-weeks, 4-weeks, and cumulative time points. Data are represented as a mean \pm standard error of the mean. *** $p < 0.001$, ($n \geq 6$ for all groups).

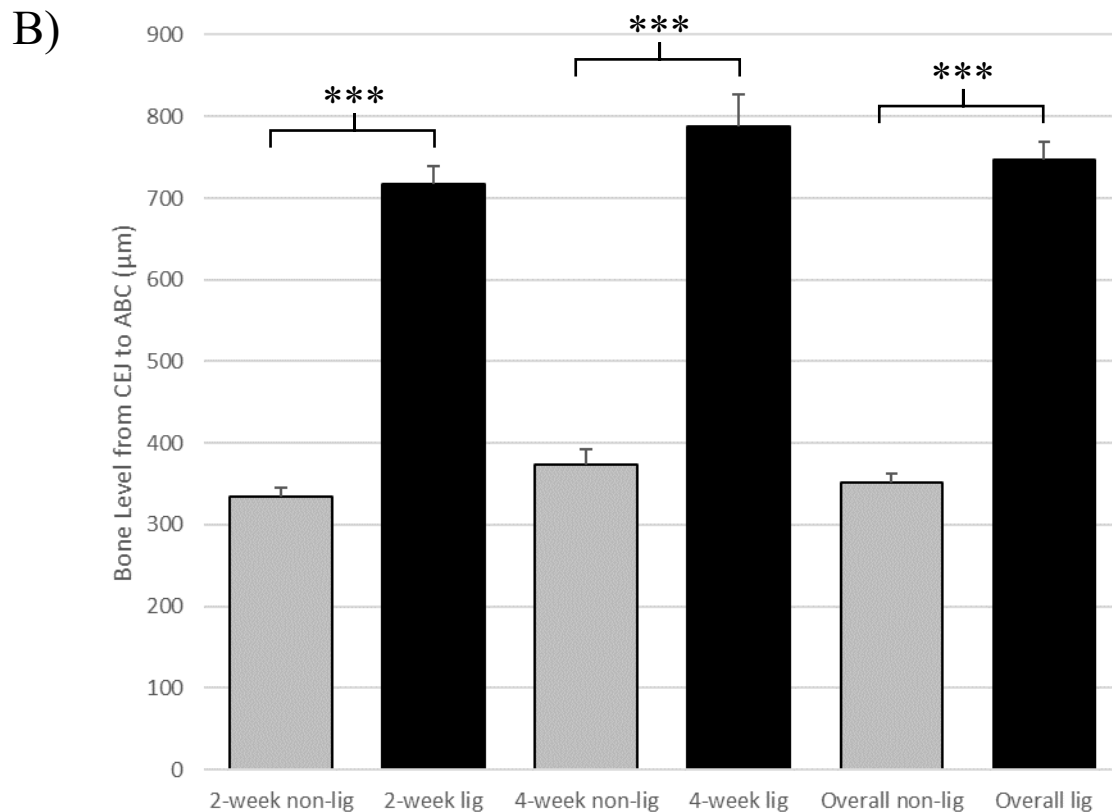
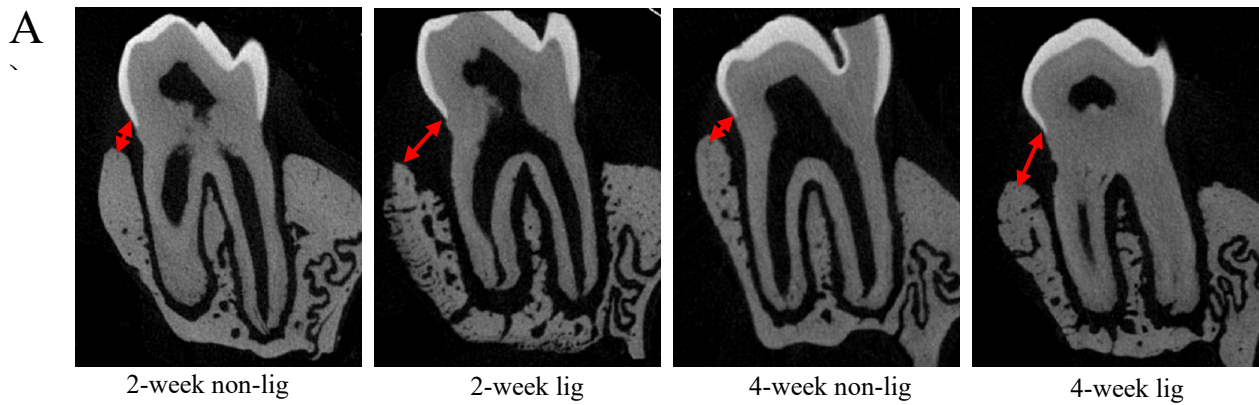
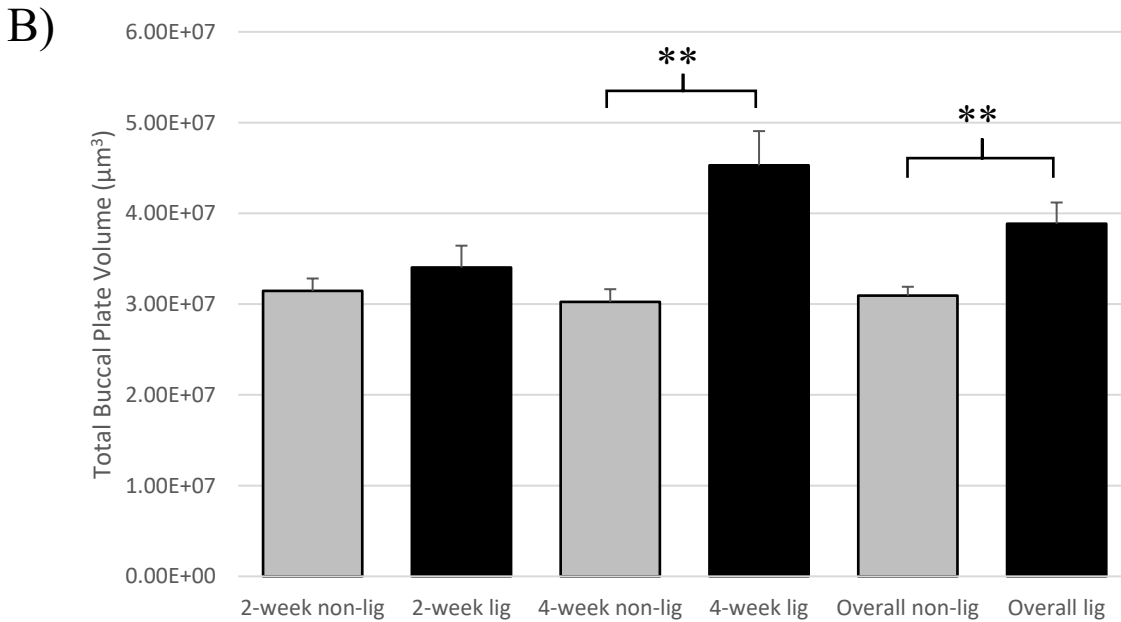
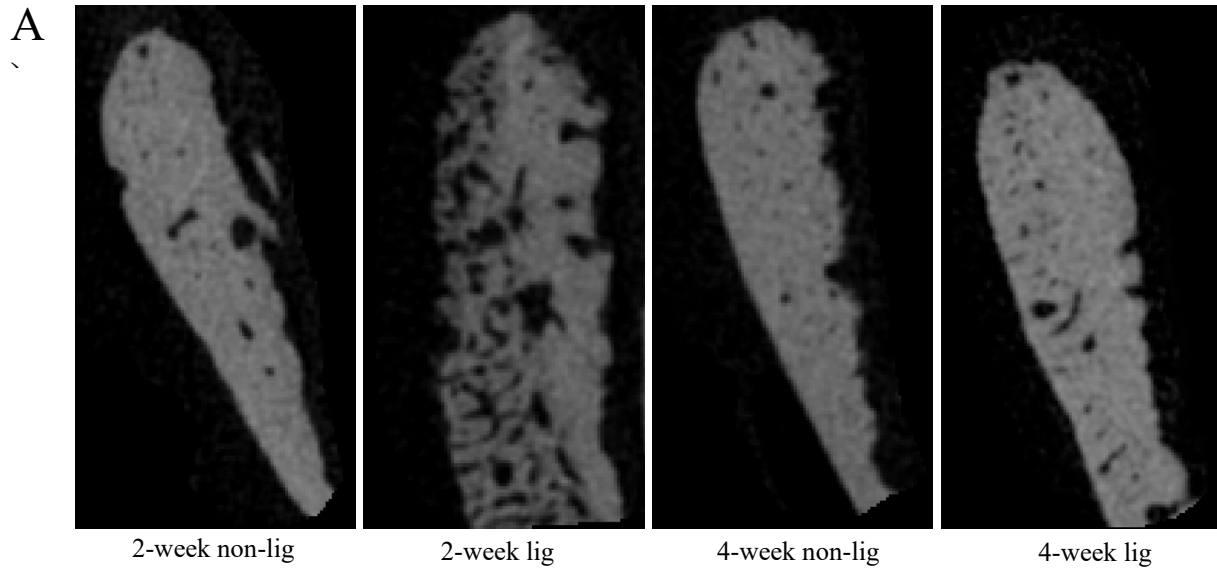


Figure 4: Radiographic analysis of buccal plate bone loss at maxillary molars **A)** Representative images of buccal bone height in a sagittal plane. **B)** Comparison of non-ligature and ligature sites at 2-weeks, 4-weeks, and cumulative time points. Data are represented as a \pm standard error of the mean. *** $p < 0.001$, ($n \geq 6$ for all groups).



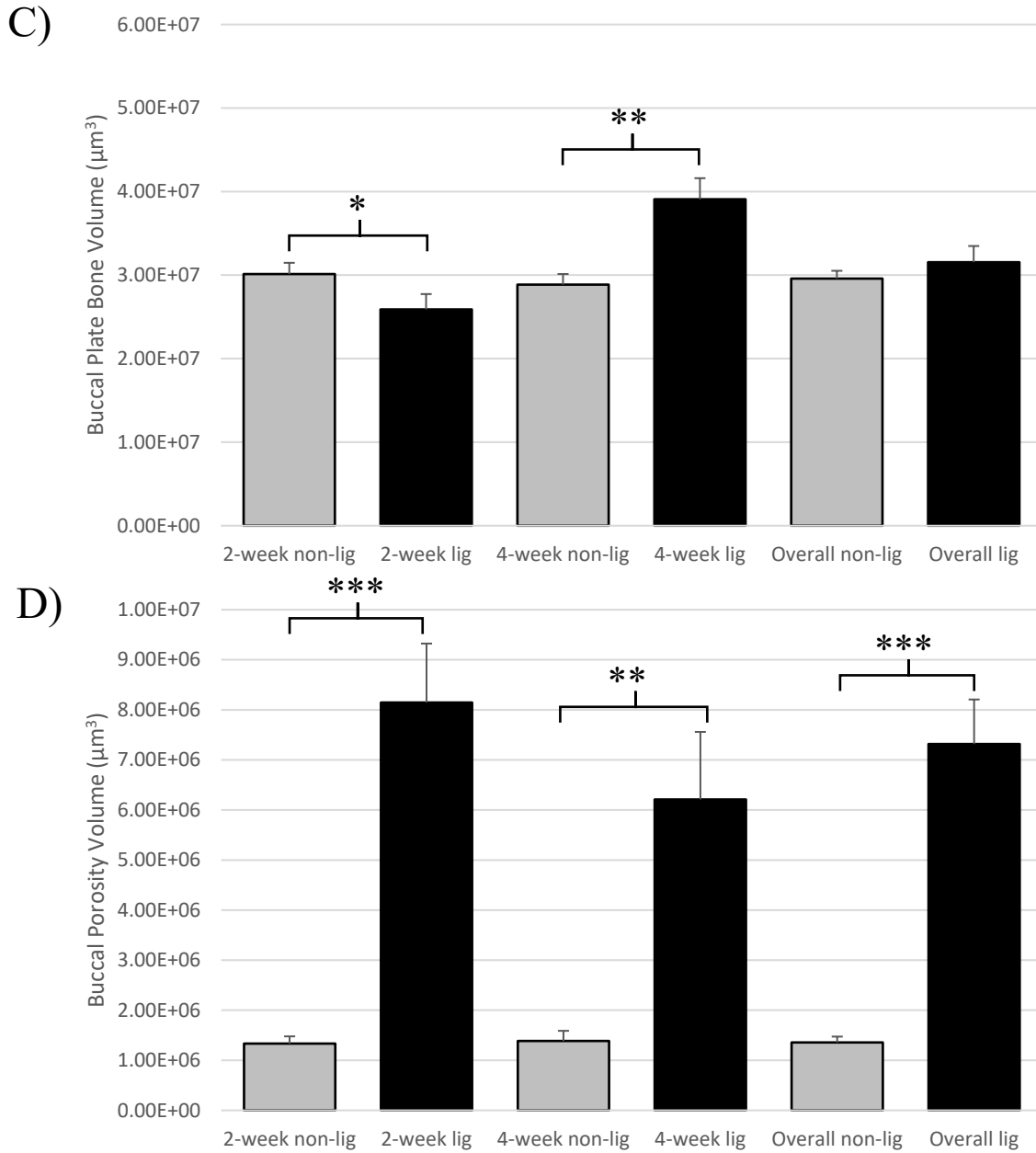


Figure 5: Analysis of radiographic bone and porosity changes in the maxillary buccal plate **A)** Representative images of buccal bone in sagittal plane. **B)** Comparison total buccal plate volume in non-ligature and ligature sites at 2-weeks, 4-weeks, and cumulative time points. **C)** Comparison of buccal plate bone volume in non-ligature and ligature sites at 2-weeks, 4-weeks, and cumulative time points. **D)** Comparison of buccal plate porosity volume in non-ligature and ligature sites at 2-weeks, 4-weeks, and cumulative time points. Data are represented as a mean \pm standard error of the mean. * $p < 0.05$, ** $p < 0.01$ *** $p < 0.001$, ($n \geq 6$ for all groups).

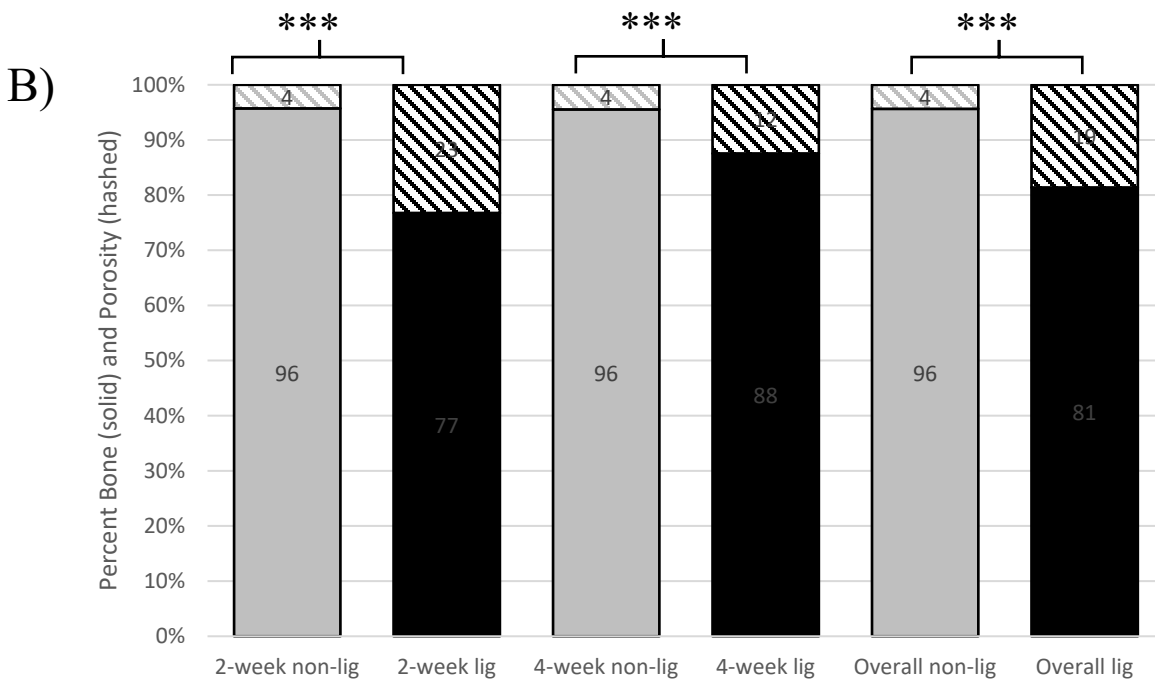
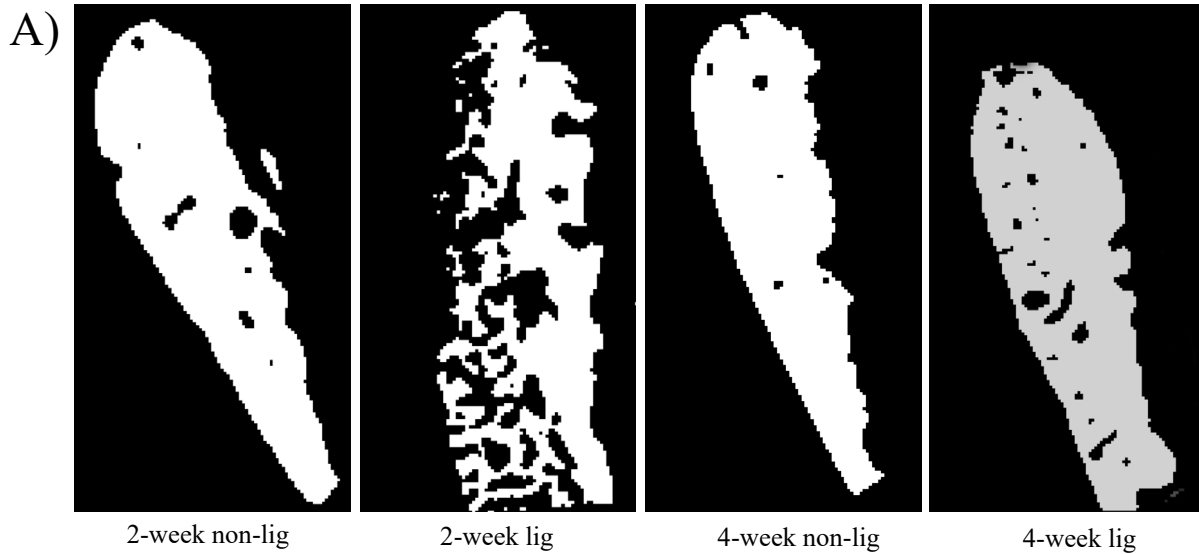


Figure 6: Proportion of maxillary buccal plate bone and porosity **A)** Representative segmentation of buccal plate bone and porosity. **B)** Analysis of mean percentage of buccal plate bone and porosity. Data are represented as a mean \pm standard error of the mean. *** $p < 0.001$, ($n \geq 6$ for all groups).

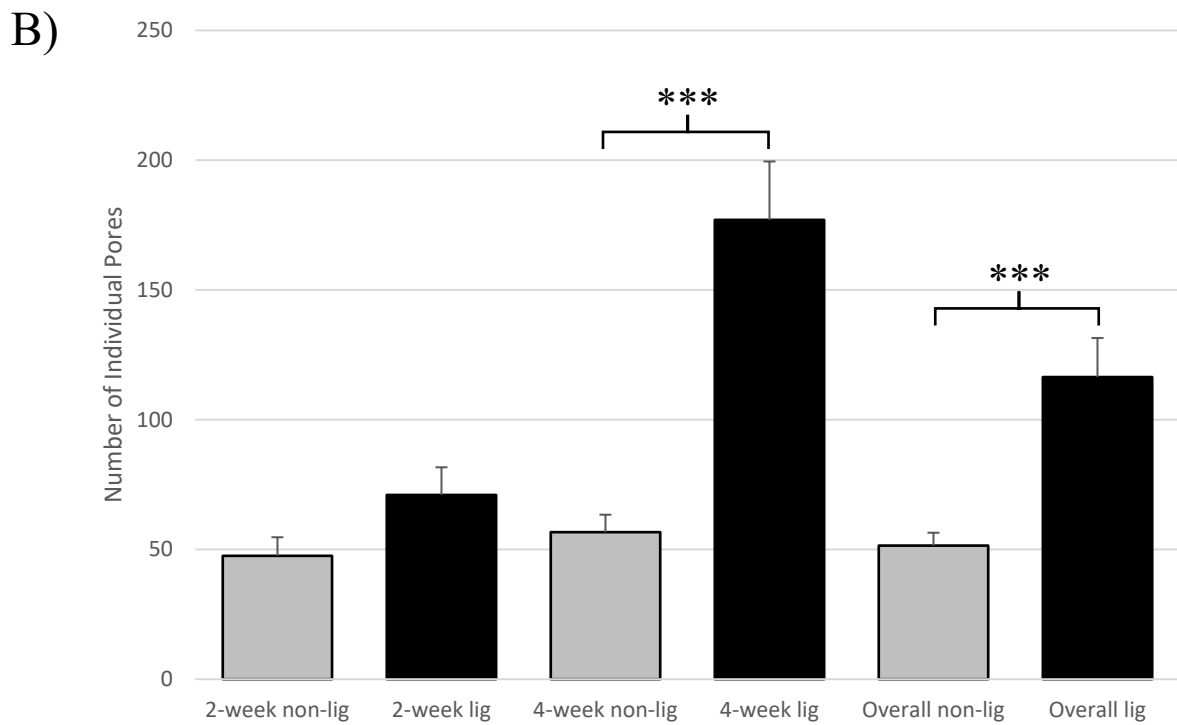
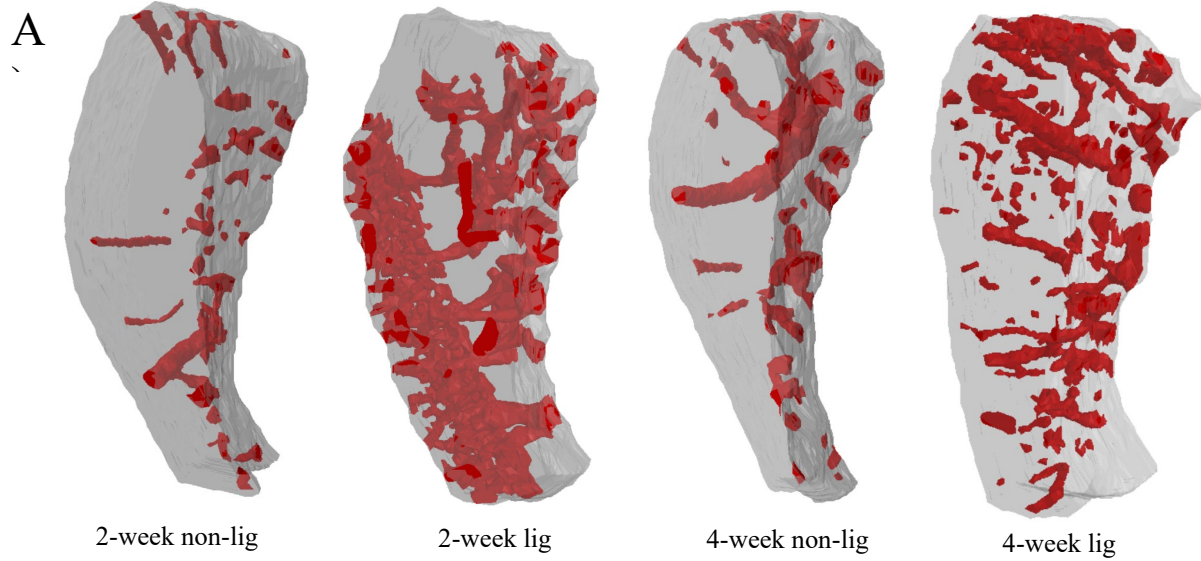


Figure 7: Number of individual maxillary buccal plate pores **A)** Representative model of segmented pores within entire buccal plate. **B)** Comparison of non-ligature and ligature sites at 2-weeks, 4-weeks, and cumulative time points. Data are represented as a mean \pm standard error of the mean. *** $p < 0.001$, ($n \geq 6$ for all groups).

A



2-week non-lig

2-week lig

4-week non-lig

4-week lig

B



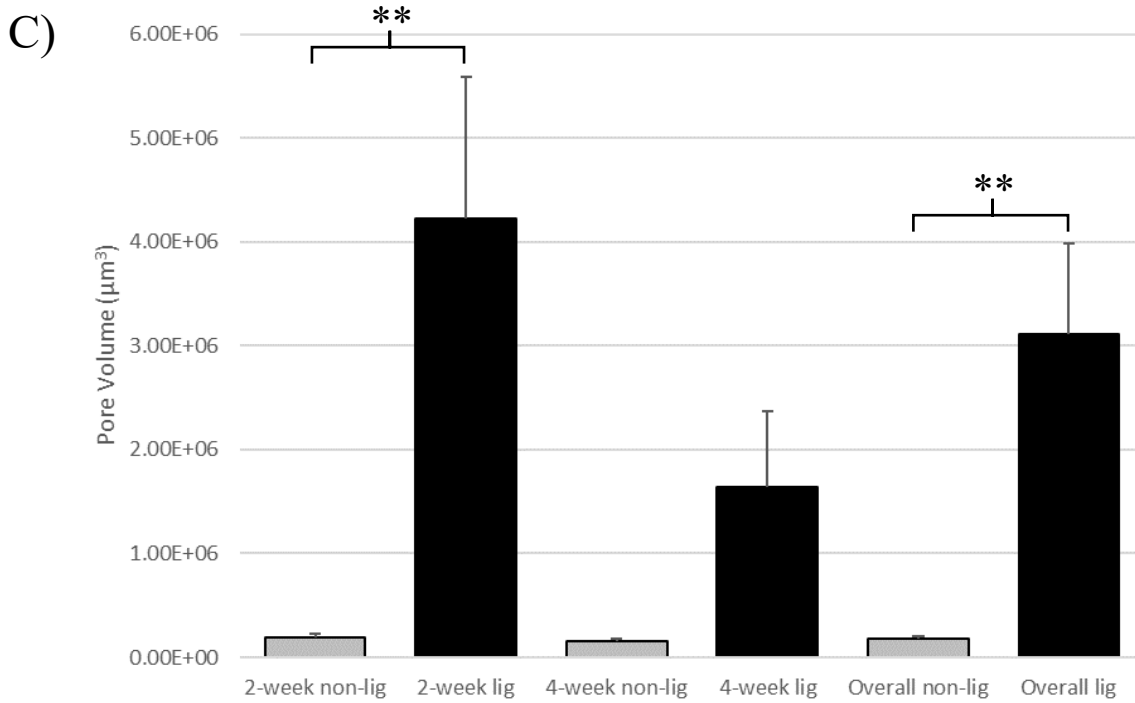


Figure 8: Average volume of individual maxillary buccal plate pores **A)** Representative model of segmented pores within entire buccal plate. **B)** Without entire segmented buccal plate, rotated view. **C)** Comparison of non-ligature and ligature sites at 2-weeks, 4-weeks, and cumulative time points. Data are represented as a mean \pm standard error of the mean. ****** $p < 0.01$, ($n \geq 6$ for all groups).

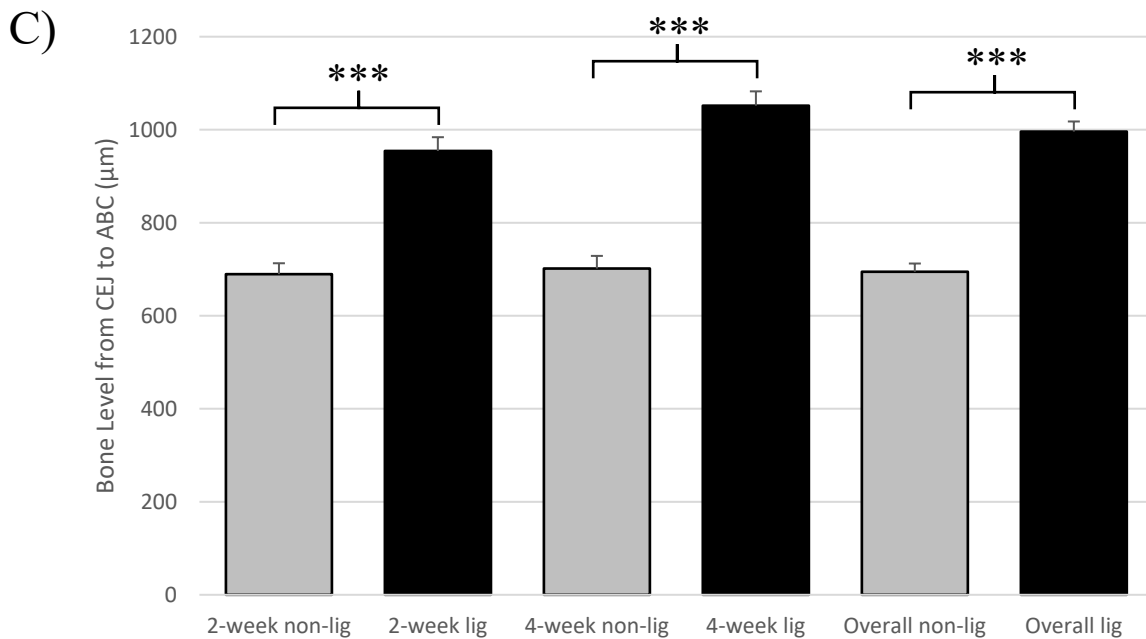
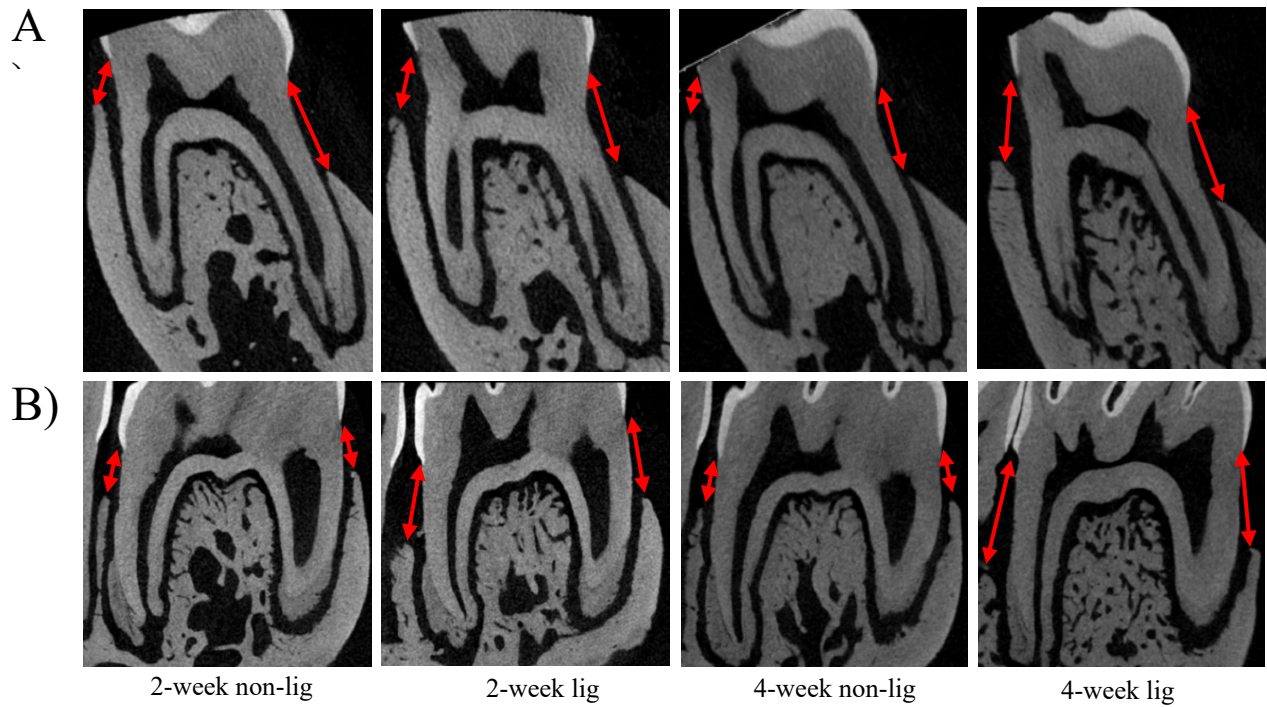
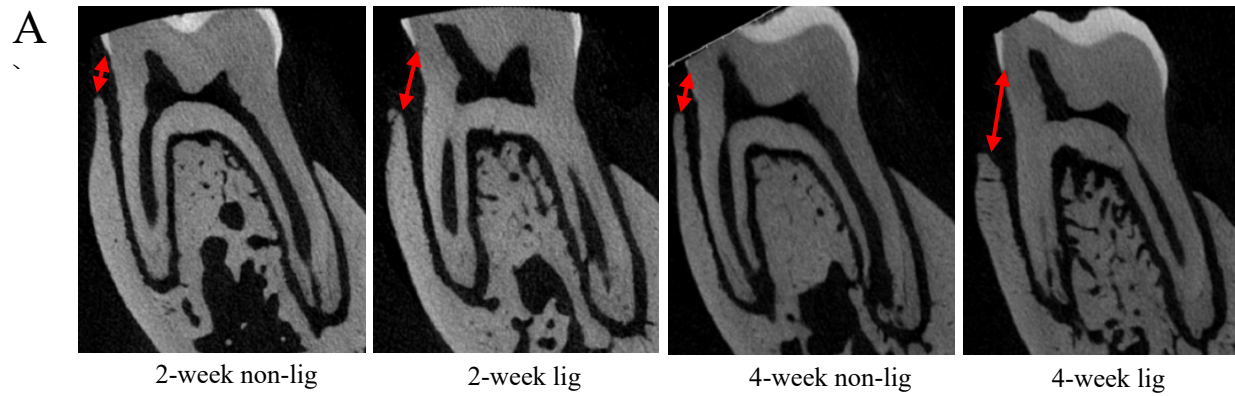


Figure 9: Radiographic analysis of bone loss measured circumferentially around mandibular molars **A)** Representative images of buccal and lingual bone height analysis in a sagittal plane. **B)** Representative images of interproximal bone height in a transverse plane. **C)** Comparison of non-ligature and ligature sites at 2-weeks, 4-weeks, and cumulative time points.

Data are represented as a mean \pm standard error of the mean. *** $p < 0.001$, ($n \geq 6$ for all groups).



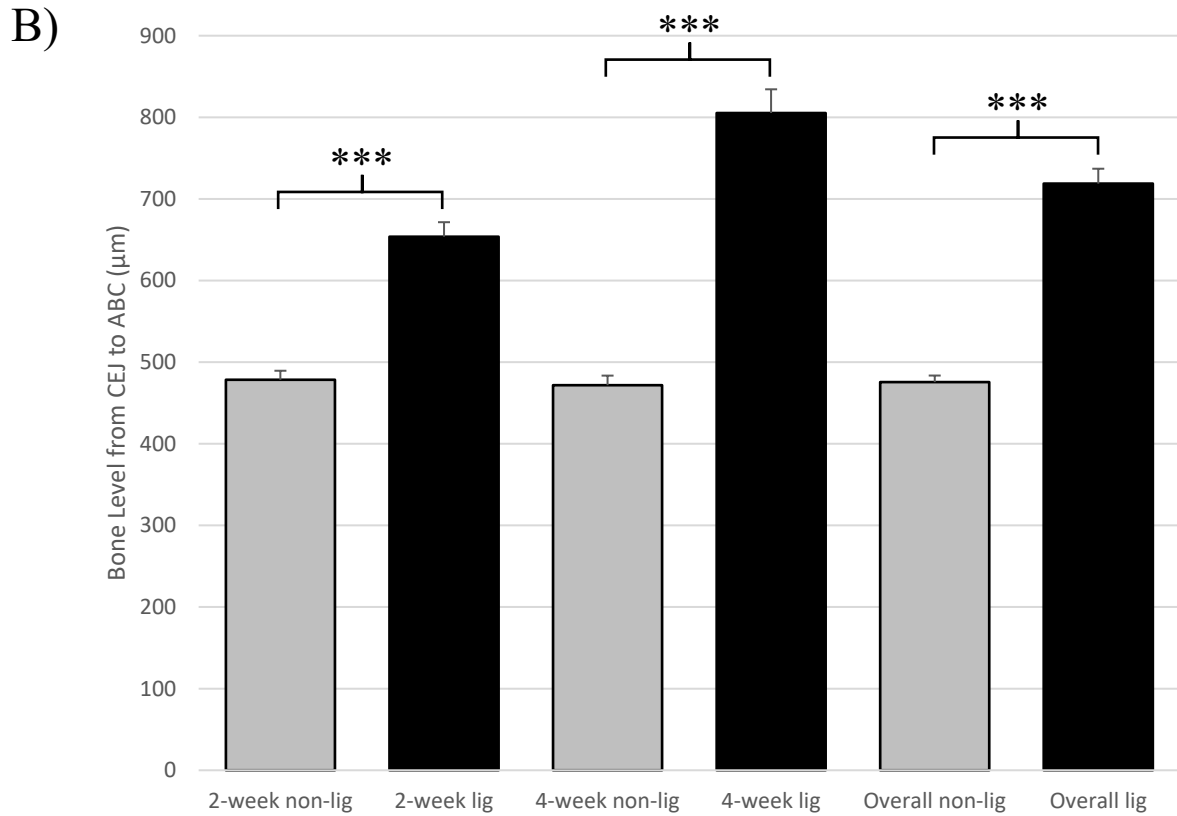
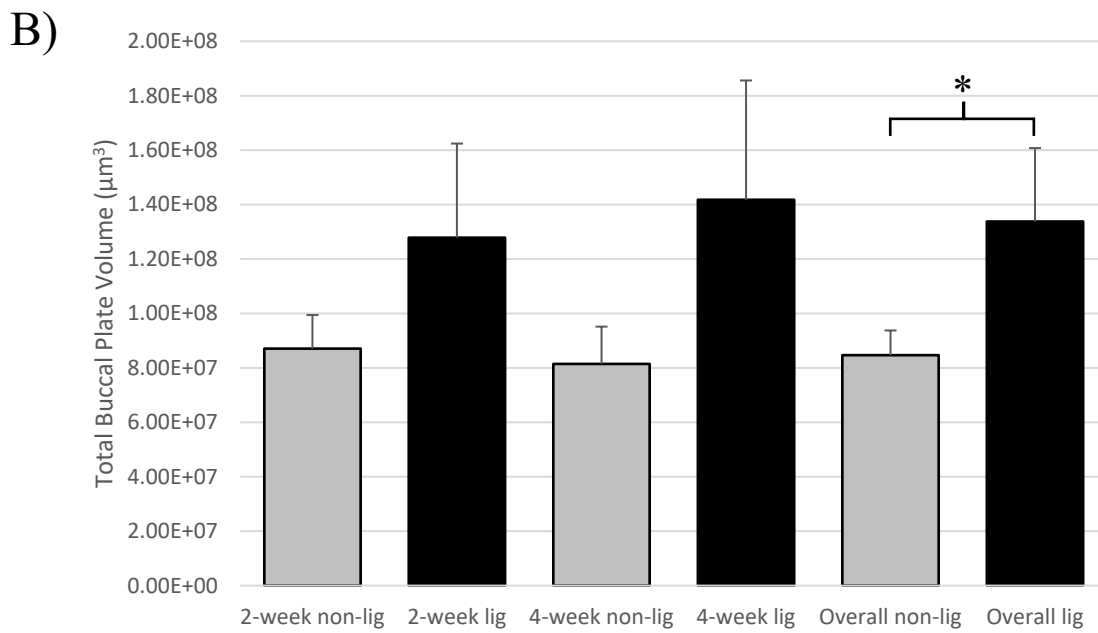
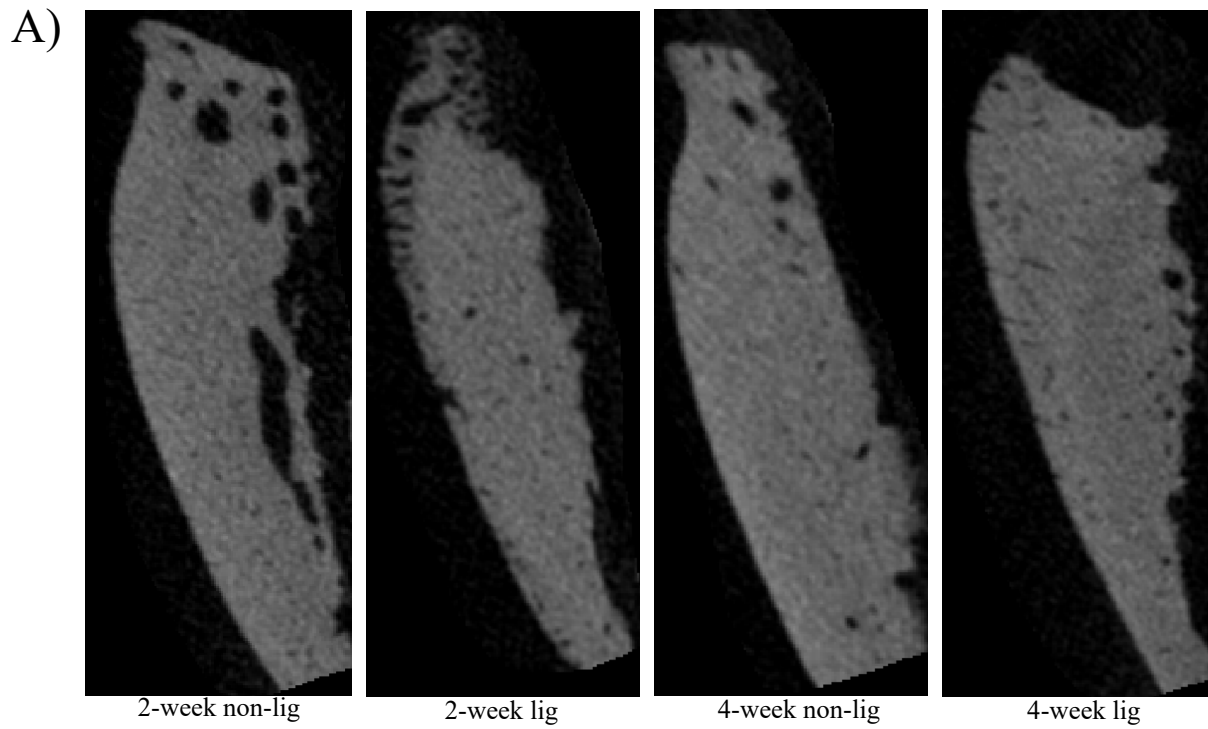


Figure 10: Radiographic analysis of buccal plate bone loss at mandibular molars **A)** Representative images of buccal bone height in a sagittal plane. **B)** Comparison of non-ligature and ligature sites at 2-weeks, 4-weeks, and cumulative time points. Data are represented as a \pm standard error of the mean. *** $p < 0.001$, ($n \geq 6$ for all groups).



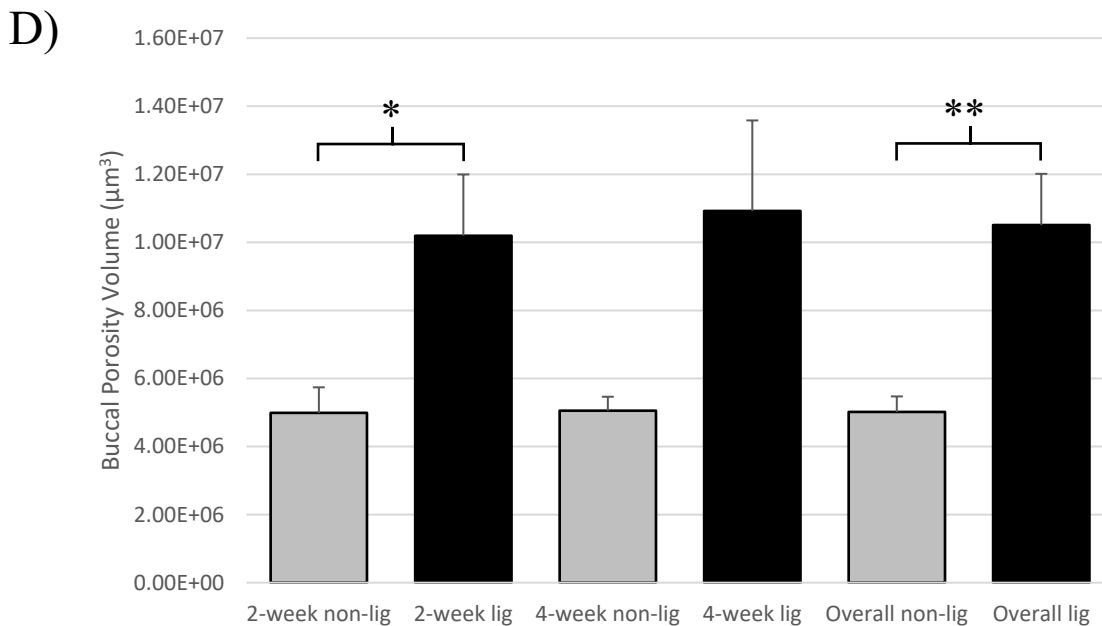
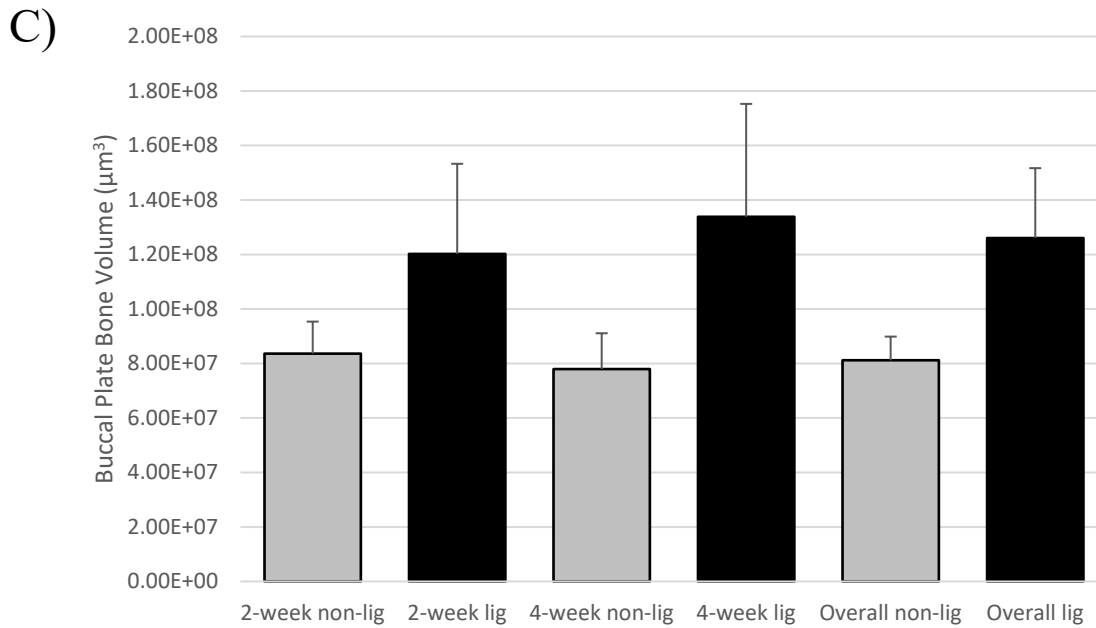


Figure 11: Analysis of radiographic bone and porosity changes in the mandibular buccal plate **A)** Representative images of buccal bone in sagittal plane. **B)** Comparison total buccal plate volume in non-ligature and ligature sites at 2-weeks, 4-weeks, and cumulative time points. **C)** Comparison of buccal plate bone volume in non-ligature and ligature sites at 2-weeks, 4-weeks, and cumulative time points. **D)** Comparison of buccal plate porosity volume in non-ligature and ligature sites at 2-weeks, 4-weeks, and

cumulative time points. Data are represented as a mean \pm standard error of the mean. * $p < 0.05$, ** $p < 0.01$, ($n \geq 6$ for all groups).

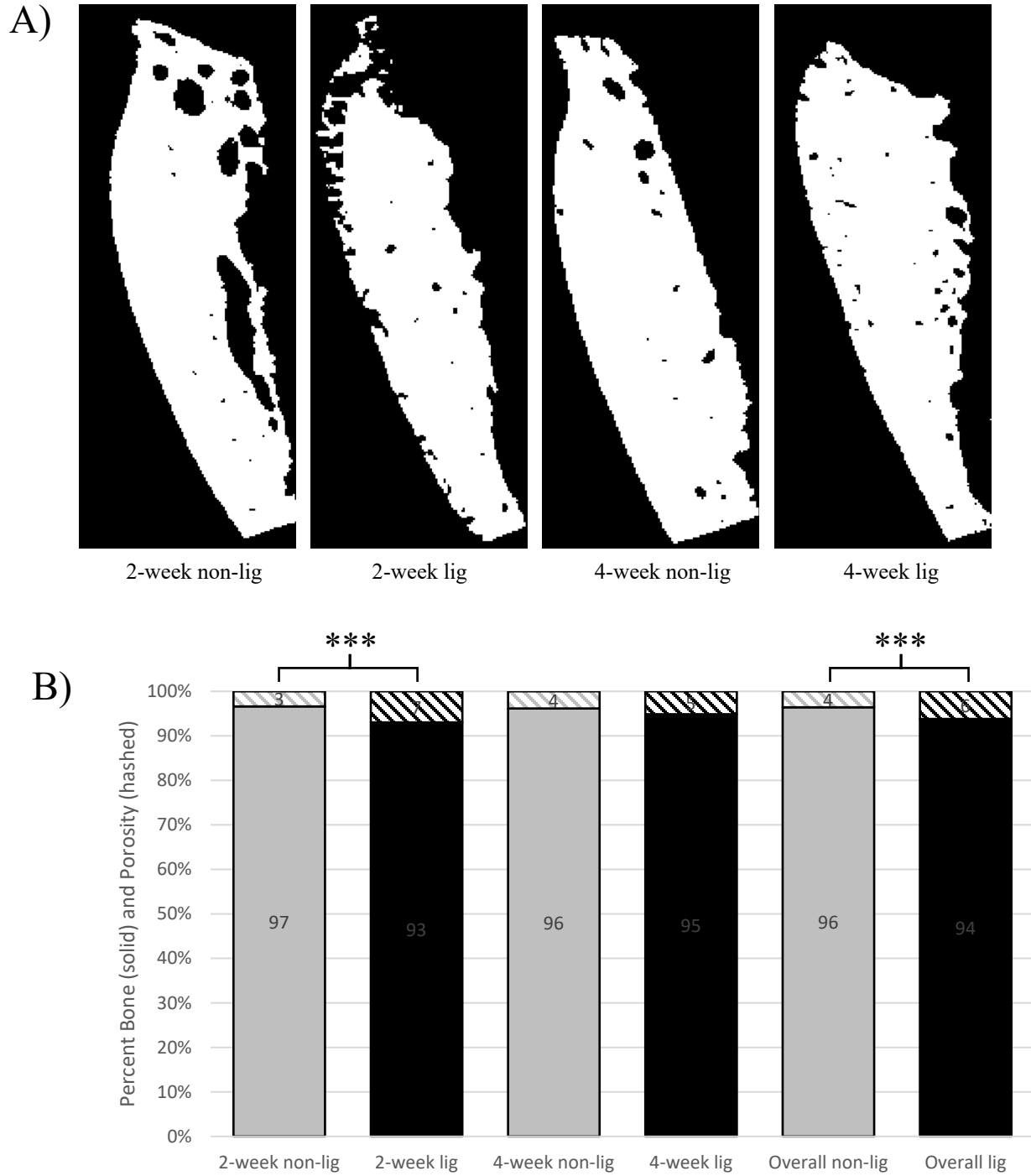


Figure 12: Proportion of mandibular buccal plate bone and porosity **A)** Representative segmentation of buccal plate bone and porosity. **B)** Analysis

of mean percentage of buccal plate bone and porosity. Data are represented as a mean \pm standard error of the mean. *** $p < 0.001$, ($n \geq 6$ for all groups).

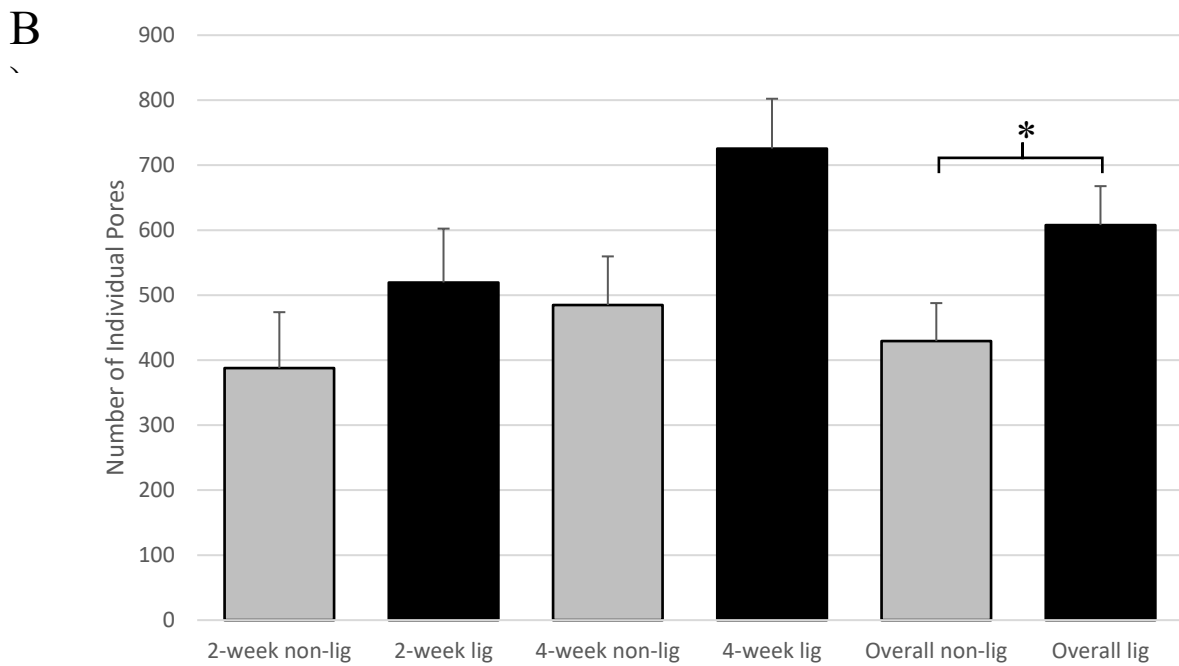
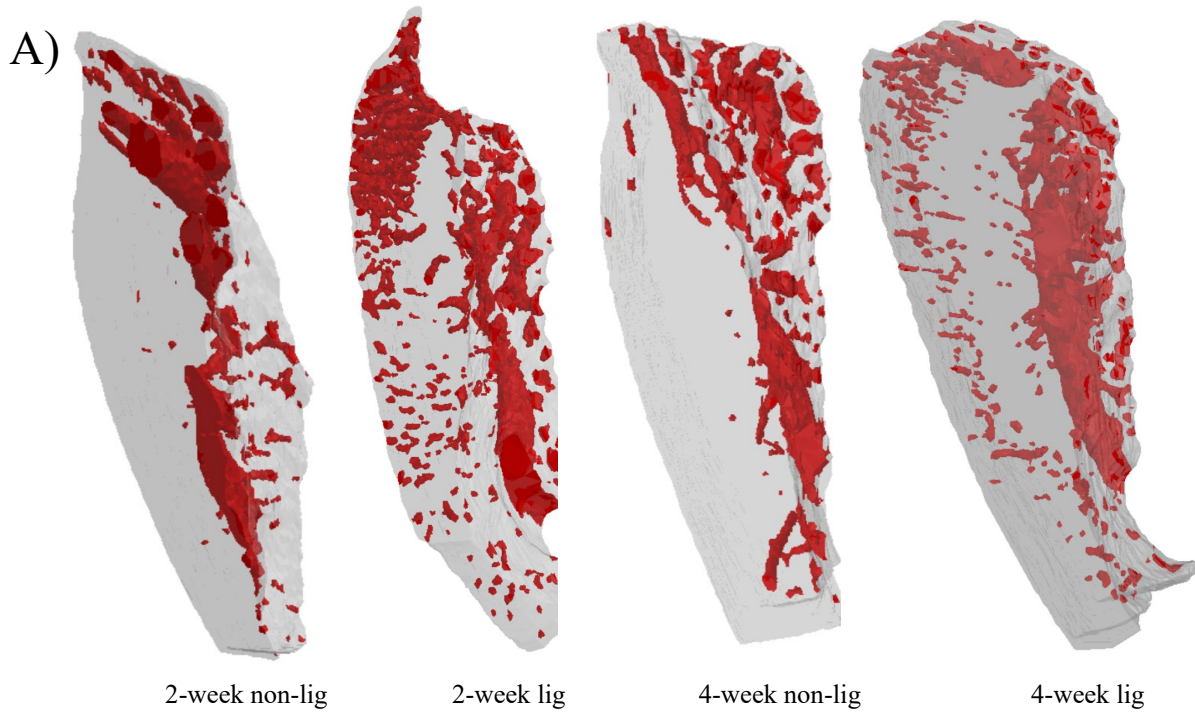
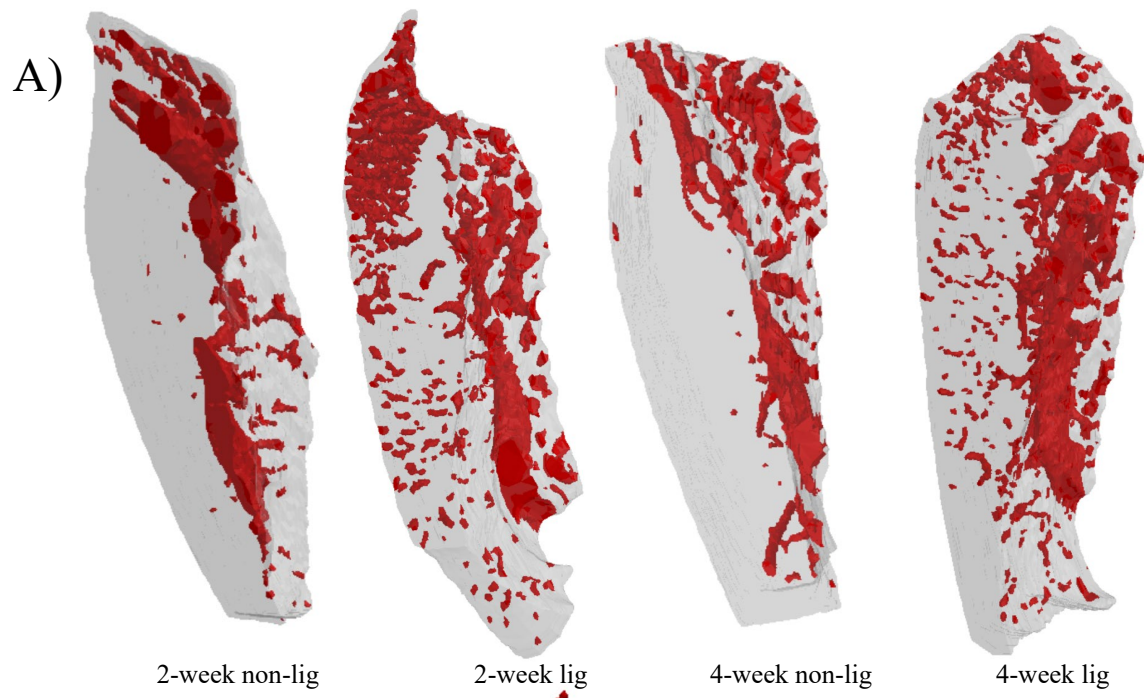


Figure 13: Number of individual mandibular buccal plate pores **A)** Representative model of segmented pores within entire buccal plate. **B)** Comparison of non-ligature and ligature sites at 2-weeks, 4-weeks, and cumulative time points. Data are represented as a mean \pm standard error of the mean. * $p < 0.05$, ($n \geq 6$ for all groups).



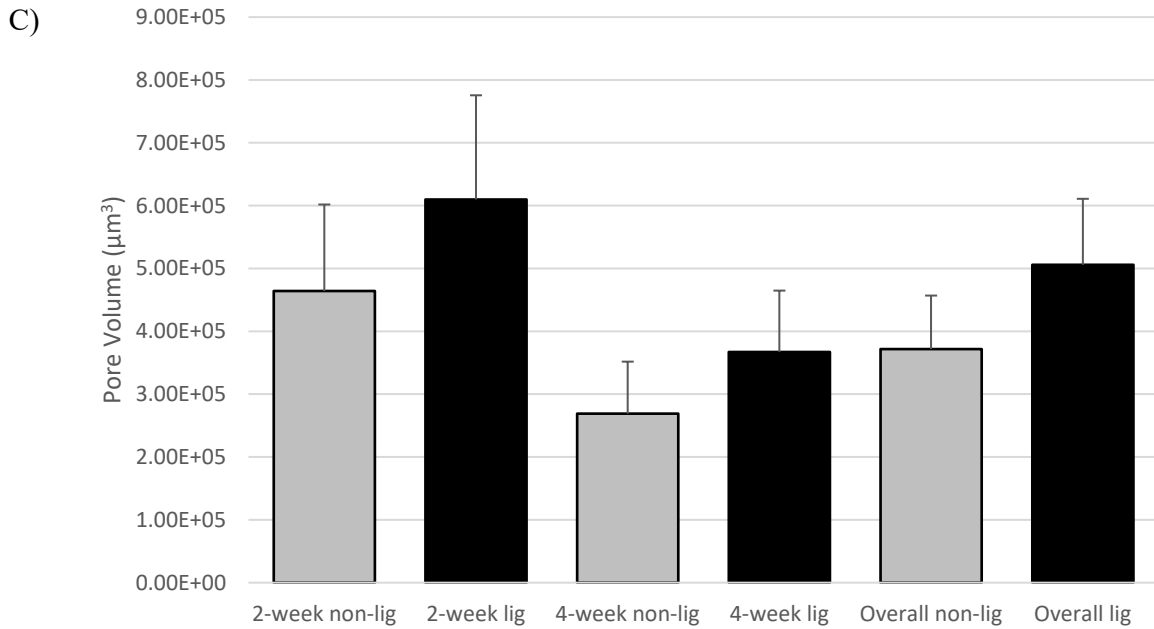


Figure 14: Average volume of individual mandibular buccal plate pores **A)** Representative model of segmented pores within entire buccal plate. **B)** Without entire segmented buccal plate, rotated view. **C)** Comparison of non-ligature and ligature sites at 2-weeks, 4-weeks, and cumulative time points. Data are represented as a mean \pm standard error of the mean. ($n \geq 6$ for all groups).

REFERENCES

- Aghaloo, T. L., Chaichanasakul, T., Bezouglaia, O., Kang, B., Franco, R., Dry, S. M., Atti, E., & Tetradis, S. (2010). Osteogenic Potential of Mandibular vs. Long-bone Marrow Stromal Cells. *Journal of Dental Research*, *89*(11), 1293–1298. <https://doi.org/10.1177/0022034510378427>
- Armitage, G. C. (1996). Periodontal Diseases: Diagnosis. *Annals of Periodontology*, *1*(1), 37–215. <https://doi.org/10.1902/annals.1996.1.1.37>
- Ascenzi, M.-G. (2012). The osteon: the micromechanical unit of compact bone. *Frontiers in Bioscience*, *17*(1), 1551. <https://doi.org/10.2741/4003>
- Asghar, A., Kumar, A., Narayan, R., & Naaz, S. (2020). Is the cortical capillary renamed as the transcortical vessel in diaphyseal vascularity? *The Anatomical Record*, *303*(11), 2774–2784. <https://doi.org/10.1002/ar.24461>
- Berendsen, A. D., & Olsen, B. R. (2015). Bone development. *Bone*, *80*, 14–18. <https://doi.org/10.1016/j.bone.2015.04.035>
- Blair, H. C., Larrouture, Q. C., Li, Y., Lin, H., Beer-Stoltz, D., Liu, L., Tuan, R. S., Robinson, L. J., Schlesinger, P. H., & Nelson, D. J. (2017). Osteoblast Differentiation and Bone Matrix Formation *In Vivo* and *In Vitro*. *Tissue Engineering Part B: Reviews*, *23*(3), 268–280. <https://doi.org/10.1089/ten.teb.2016.0454>
- Bonewald, L. F. (2011). The amazing osteocyte. *Journal of Bone and Mineral Research*, *26*(2), 229–238. <https://doi.org/10.1002/jbmr.320>
- BRITZ, H. M., JOKIHAARA, J., LEPPÄNEN, O. V., JÄRVINEN, T., & COOPER, D. M. L. (2010). 3D visualization and quantification of rat cortical bone porosity using a desktop micro-CT system: a case study in the tibia. *Journal of Microscopy*, *240*(1), 32–37. <https://doi.org/10.1111/j.1365-2818.2010.03381.x>
- Carulli, C., Innocenti, M., & Brandi, M. L. (2013). Bone Vascularization in Normal and Disease Conditions. *Frontiers in Endocrinology*, *4*. <https://doi.org/10.3389/fendo.2013.00106>
- Chappuis, V., Araújo, M. G., & Buser, D. (2017). Clinical relevance of dimensional bone and soft tissue alterations post-extraction in esthetic sites. *Periodontology 2000*, *73*(1), 73–83. <https://doi.org/10.1111/prd.12167>
- Clarke, B. (2008). Normal Bone Anatomy and Physiology. *Clinical Journal of the American Society of Nephrology*, *3*(Supplement 3), S131–S139. <https://doi.org/10.2215/CJN.04151206>
- Cooper, D. M. L., Erickson, B., Peele, A. G., Hannah, K., Thomas, C. D. L., & Clement, J. G. (2011). Visualization of 3D osteon morphology by synchrotron radiation micro-CT. *Journal of Anatomy*, *219*(4), 481–489. <https://doi.org/10.1111/j.1469-7580.2011.01398.x>

- Cooper, D. M. L., Matyas, J. R., Katzenberg, M. A., & Hallgrímsson, B. (2004). Comparison of Microcomputed Tomographic and Microradiographic Measurements of Cortical Bone Porosity. *Calcified Tissue International*, *74*(5), 437–447. <https://doi.org/10.1007/s00223-003-0071-z>
- Cooper, D. M. L., Thomas, C. D. L., Clement, J. G., & Hallgrímsson, B. (2006). Three-dimensional microcomputed tomography imaging of basic multicellular unit-related resorption spaces in human cortical bone. *The Anatomical Record Part A: Discoveries in Molecular, Cellular, and Evolutionary Biology*, *288A*(7), 806–816. <https://doi.org/10.1002/ar.a.20344>
- Cooper, D. M. L., Turinsky, A. L., Sensen, C. W., & Hallgrímsson, B. (2003). Quantitative 3D analysis of the canal network in cortical bone by micro-computed tomography. *The Anatomical Record Part B: The New Anatomist*, *274B*(1), 169–179. <https://doi.org/10.1002/ar.b.10024>
- Cooper, D., Turinsky, A., Sensen, C., & Hallgrímsson, B. (2007). Effect of Voxel Size on 3D Micro-CT Analysis of Cortical Bone Porosity. *Calcified Tissue International*, *80*(3), 211–219. <https://doi.org/10.1007/s00223-005-0274-6>
- Eke, P. I., Dye, B. A., Wei, L., Slade, G. D., Thornton-Evans, G. O., Borgnakke, W. S., Taylor, G. W., Page, R. C., Beck, J. D., & Genco, R. J. (2015). Update on Prevalence of Periodontitis in Adults in the United States: NHANES 2009 to 2012. *Journal of Periodontology*, *86*(5), 611–622. <https://doi.org/10.1902/jop.2015.140520>
- Enlow, D. H. (1962). Functions of the haversian system. *American Journal of Anatomy*, *110*(3), 269–305. <https://doi.org/10.1002/aja.1001100305>
- Eriksen, E. F. (2010). Cellular mechanisms of bone remodeling. *Reviews in Endocrine and Metabolic Disorders*, *11*(4), 219–227. <https://doi.org/10.1007/s11154-010-9153-1>
- Grassi, F. R., Grassi, R., Rapone, B., Alemanno, G., Balena, A., & Kalemaj, Z. (2019). Dimensional changes of buccal bone plate in immediate implants inserted through open flap, open flap and bone grafting and flapless techniques: A cone-beam computed tomography randomized controlled clinical trial. *Clinical Oral Implants Research*, *30*(12), 1155–1164. <https://doi.org/10.1111/clr.13528>
- Grüneboom, A., Hawwari, I., Weidner, D., Culemann, S., Müller, S., Henneberg, S., Brenzel, A., Merz, S., Bornemann, L., Zec, K., Wuelling, M., Kling, L., Hasenberg, M., Voortmann, S., Lang, S., Baum, W., Ohs, A., Kraff, O., Quick, H. H., ... Gunzer, M. (2019). A network of trans-cortical capillaries as mainstay for blood circulation in long bones. *Nature Metabolism*, *1*(2), 236–250. <https://doi.org/10.1038/s42255-018-0016-5>
- Hajishengallis, G. (2015). Periodontitis: from microbial immune subversion to systemic inflammation. *Nature Reviews Immunology*, *15*(1), 30–44. <https://doi.org/10.1038/nri3785>

- Hendriks, M., & Ramasamy, S. K. (2020). Blood Vessels and Vascular Niches in Bone Development and Physiological Remodeling. *Frontiers in Cell and Developmental Biology*, 8. <https://doi.org/10.3389/fcell.2020.602278>
- Heřt, J., Fiala, P., & Petrtýl, M. (1994). Osteon orientation of the diaphysis of the long bones in man. *Bone*, 15(3), 269–277. [https://doi.org/10.1016/8756-3282\(94\)90288-7](https://doi.org/10.1016/8756-3282(94)90288-7)
- Iezzi, G., Mangano, C., Barone, A., Tirone, F., Baggi, L., Tromba, G., Piattelli, A., & Giuliani, A. (2020). Jawbone remodeling: a conceptual study based on Synchrotron High-resolution Tomography. *Scientific Reports*, 10(1), 3777. <https://doi.org/10.1038/s41598-020-60718-8>
- Intemann, J., de Gorter, D. J. J., Naylor, A. J., Dankbar, B., & Wehmeyer, C. (2020). Importance of osteocyte-mediated regulation of bone remodelling in inflammatory bone disease. *Swiss Medical Weekly*. <https://doi.org/10.4414/smw.2020.20187>
- Jast, J., & Jasiuk, I. (2013). Age-related changes in the 3D hierarchical structure of rat tibia cortical bone characterized by high-resolution micro-CT. *Journal of Applied Physiology*, 114(7), 923–933. <https://doi.org/10.1152/jappphysiol.00948.2011>
- Kim, J.-M., Lin, C., Stavre, Z., Greenblatt, M. B., & Shim, J.-H. (2020). Osteoblast-Osteoclast Communication and Bone Homeostasis. *Cells*, 9(9), 2073. <https://doi.org/10.3390/cells9092073>
- Kim, J.-N., Lee, J.-Y., Shin, K.-J., Gil, Y.-C., Koh, K.-S., & Song, W.-C. (2015). Haversian system of compact bone and comparison between endosteal and periosteal sides using three-dimensional reconstruction in rat. *Anatomy & Cell Biology*, 48(4), 258. <https://doi.org/10.5115/acb.2015.48.4.258>
- Kim, Y., Roh, B.-D., Shin, Y., Kim, B. S., Choi, Y., & Ha, A. (2018). Morphological Characteristics and Classification of Mandibular First Molars Having 2 Distal Roots or Canals: 3-Dimensional Biometric Analysis Using Cone-beam Computed Tomography in a Korean Population. *Journal of Endodontics*, 44(1), 46–50. <https://doi.org/10.1016/j.joen.2017.08.005>
- Kishi, K., Nagaoka, T., Gotoh, T., Imai, K., & Fujiki, Y. (1982). Radiographic study of mandibular nutrient canals. *Oral Surgery, Oral Medicine, Oral Pathology*, 54(1), 118–122. [https://doi.org/10.1016/0030-4220\(82\)90426-1](https://doi.org/10.1016/0030-4220(82)90426-1)
- Kusumbe, A. P., Ramasamy, S. K., & Adams, R. H. (2014). Coupling of angiogenesis and osteogenesis by a specific vessel subtype in bone. *Nature*, 507(7492), 323–328. <https://doi.org/10.1038/nature13145>
- Lafage-Proust, M.-H., Roche, B., Langer, M., Cleret, D., vanden Bossche, A., Olivier, T., & Vico, L. (2015). Assessment of bone vascularization and its role in bone remodeling. *BoneKey Reports*, 4. <https://doi.org/10.1038/bonekey.2015.29>
- Marenzana, M., & Arnett, T. R. (2013). The Key Role of the Blood Supply to Bone. *Bone Research*, 1(3), 203–215. <https://doi.org/10.4248/BR201303001>

- Martín-Badosa, E., Amblard, D., Nuzzo, S., Elmoutaouakkil, A., Vico, L., & Peyrin, F. (2003). Excised Bone Structures in Mice: Imaging at Three-dimensional Synchrotron Radiation Micro CT. *Radiology*, *229*(3), 921–928. <https://doi.org/10.1148/radiol.2293020558>
- McLean, T. N., Smith, B. A., Morrison, E. C., Nasjleti, C. E., & Caffesse, R. G. (1995). Vascular Changes Following Mucoperiosteal Flap Surgery: A Fluorescein Angiography Study in Dogs. *Journal of Periodontology*, *66*(3), 205–210. <https://doi.org/10.1902/jop.1995.66.3.205>
- Metz, L. N., Martin, R. B., & Turner, A. S. (2003). Histomorphometric analysis of the effects of osteocyte density on osteonal morphology and remodeling. *Bone*, *33*(5), 753–759. [https://doi.org/10.1016/S8756-3282\(03\)00245-X](https://doi.org/10.1016/S8756-3282(03)00245-X)
- Metzger, C. E., & Narayanan, S. A. (2019). The Role of Osteocytes in Inflammatory Bone Loss. *Frontiers in Endocrinology*, *10*. <https://doi.org/10.3389/fendo.2019.00285>
- Moskow, B. S., Tannenbaum, P., & Bloom, A. (1985). Visualization of the Human Periodontium Using Serial Thin Section Contact Radiography. *Journal of Periodontology*, *56*(4), 223–233. <https://doi.org/10.1902/jop.1985.56.4.223>
- Núñez, J. A., Goring, A., Hesse, E., Thurner, P. J., Schneider, P., & Clarkin, C. E. (2017). Simultaneous visualisation of calcified bone microstructure and intracortical vasculature using synchrotron X-ray phase contrast-enhanced tomography. *Scientific Reports*, *7*(1), 13289. <https://doi.org/10.1038/s41598-017-13632-5>
- O'Brien, C. A., Plotkin, L. I., Galli, C., Goellner, J. J., Gortazar, A. R., Allen, M. R., Robling, A. G., Bouxsein, M., Schipani, E., Turner, C. H., Jilka, R. L., Weinstein, R. S., Manolagas, S. C., & Bellido, T. (2008). Control of Bone Mass and Remodeling by PTH Receptor Signaling in Osteocytes. *PLoS ONE*, *3*(8), e2942. <https://doi.org/10.1371/journal.pone.0002942>
- Oftadeh, R., Perez-Viloria, M., Villa-Camacho, J. C., Vaziri, A., & Nazarian, A. (2015). Biomechanics and Mechanobiology of Trabecular Bone: A Review. *Journal of Biomechanical Engineering*, *137*(1). <https://doi.org/10.1115/1.4029176>
- Palacio-Manchero, P. E., Larriera, A. I., Doty, S. B., Cardoso, L., & Fritton, S. P. (2014). 3D Assessment of Cortical Bone Porosity and Tissue Mineral Density Using High-Resolution μ CT: Effects of Resolution and Threshold Method. *Journal of Bone and Mineral Research*, *29*(1), 142–150. <https://doi.org/10.1002/jbmr.2012>
- Pawelczyk-Madalińska, M., Benedicenti, S., Sălăgean, T., Bordea, I. R., & Hanna, R. (2021). Impact of Adjunctive Diode Laser Application to Non-Surgical Periodontal Therapy on Clinical, Microbiological and Immunological Outcomes in Management of Chronic Periodontitis: A Systematic Review of Human Randomized Controlled Clinical Trials. *Journal of Inflammation Research*, *Volume 14*, 2515–2545. <https://doi.org/10.2147/JIR.S304946>

- Pazzaglia, U. E., Congiu, T., Raspanti, M., Ranchetti, F., & Quacci, D. (2009). Anatomy of the Intracortical Canal System: Scanning Electron Microscopy Study in Rabbit Femur. *Clinical Orthopaedics & Related Research*, 467(9), 2446–2456. <https://doi.org/10.1007/s11999-009-0806-x>
- Petrtyl, M., Heřt, J., & Fiala, P. (1996). Spatial organization of the haversian bone in man. *Journal of Biomechanics*, 29(2), 161–169. [https://doi.org/10.1016/0021-9290\(94\)00035-2](https://doi.org/10.1016/0021-9290(94)00035-2)
- Pihlstrom, B. L., Michalowicz, B. S., & Johnson, N. W. (2005). Periodontal diseases. *The Lancet*, 366(9499), 1809–1820. [https://doi.org/10.1016/S0140-6736\(05\)67728-8](https://doi.org/10.1016/S0140-6736(05)67728-8)
- Qing, H., Ardeshirpour, L., Divieti Pajevic, P., Dusevich, V., Jähn, K., Kato, S., Wysolmerski, J., & Bonewald, L. F. (2012). Demonstration of osteocytic perilacunar/canalicular remodeling in mice during lactation. *Journal of Bone and Mineral Research*, 27(5), 1018–1029. <https://doi.org/10.1002/jbmr.1567>
- Root, S. H., Wee, N. K. Y., Novak, S., Rosen, C. J., Baron, R., Matthews, B. G., & Kalajzic, I. (2020). Perivascular osteoprogenitors are associated with transcortical channels of long bones. *Stem Cells*, 38(6), 769–781. <https://doi.org/10.1002/stem.3159>
- Schipani, E., Maes, C., Carmeliet, G., & Semenza, G. L. (2009). Regulation of Osteogenesis-Angiogenesis Coupling by HIFs and VEGF. *Journal of Bone and Mineral Research*, 24(8), 1347–1353. <https://doi.org/10.1359/jbmr.090602>
- Schneider, P., Stauber, M., Voide, R., Stampanoni, M., Donahue, L. R., & Müller, R. (2007). Ultrastructural Properties in Cortical Bone Vary Greatly in Two Inbred Strains of Mice as Assessed by Synchrotron Light Based Micro- and Nano-CT. *Journal of Bone and Mineral Research*, 22(10), 1557–1570. <https://doi.org/10.1359/jbmr.070703>
- Schneider, P., Voide, R., Stampanoni, M., Donahue, L. R., & Müller, R. (2013). The importance of the intracortical canal network for murine bone mechanics. *Bone*, 53(1), 120–128. <https://doi.org/10.1016/j.bone.2012.11.024>
- Sietsema, W. K. (1995). Animal models of cortical porosity. *Bone*, 17(4), S297–S305. [https://doi.org/10.1016/8756-3282\(95\)00307-Y](https://doi.org/10.1016/8756-3282(95)00307-Y)
- SILVA, N., ABUSLEME, L., BRAVO, D., DUTZAN, N., GARCIA-SESNICH, J., VERNAL, R., HERNÁNDEZ, M., & GAMONAL, J. (2015). Host response mechanisms in periodontal diseases. *Journal of Applied Oral Science*, 23(3), 329–355. <https://doi.org/10.1590/1678-775720140259>
- Tanaka, M., Yamashita, E., Anwar, R. B., Yamada, K., Ohshima, H., Nomura, S., & Ejiri, S. (2011). Radiological and histologic studies of the mandibular cortex of ovariectomized monkeys. *Oral Surgery, Oral Medicine, Oral Pathology, Oral Radiology, and Endodontology*, 111(3), 372–380. <https://doi.org/10.1016/j.tripleo.2010.12.003>

- Taylor, J. J., Preshaw, P. M., & Lalla, E. (2013). A review of the evidence for pathogenic mechanisms that may link periodontitis and diabetes. *Journal of Clinical Periodontology*, *40*, S113–S134. <https://doi.org/10.1111/jcpe.12059>
- Torreggiani, E., Matthews, B. G., Pejda, S., Matic, I., Horowitz, M. C., Grcevic, D., & Kalajzic, I. (2013). Preosteocytes/Osteocytes Have the Potential to Dedifferentiate Becoming a Source of Osteoblasts. *PLoS ONE*, *8*(9), e75204. <https://doi.org/10.1371/journal.pone.0075204>
- Weiner, S., Traub, W., & Wagner, H. D. (1999). Lamellar Bone: Structure–Function Relations. *Journal of Structural Biology*, *126*(3), 241–255. <https://doi.org/10.1006/jsbi.1999.4107>
- Werner, D., Simon, D., Englbrecht, M., Stemmler, F., Simon, C., Berlin, A., Haschka, J., Renner, N., Buder, T., Engelke, K., Hueber, A. J., Rech, J., Schett, G., & Kleyer, A. (2017). Early Changes of the Cortical Micro-Channel System in the Bare Area of the Joints of Patients With Rheumatoid Arthritis. *Arthritis & Rheumatology*, *69*(8), 1580–1587. <https://doi.org/10.1002/art.40148>
- Yan, Y., Wang, L., Ge, L., & Pathak, J. L. (2020). Osteocyte-Mediated Translation of Mechanical Stimuli to Cellular Signaling and Its Role in Bone and Non-bone-Related Clinical Complications. *Current Osteoporosis Reports*, *18*(1), 67–80. <https://doi.org/10.1007/s11914-020-00564-9>
- Yee, C. S., Schurman, C. A., White, C. R., & Alliston, T. (2019). Investigating Osteocytic Perilacunar/Canalicular Remodeling. *Current Osteoporosis Reports*, *17*(4), 157–168. <https://doi.org/10.1007/s11914-019-00514-0>
- Zimmermann, E. A., Schaible, E., Bale, H., Barth, H. D., Tang, S. Y., Reichert, P., Busse, B., Alliston, T., Ager, J. W., & Ritchie, R. O. (2011). Age-related changes in the plasticity and toughness of human cortical bone at multiple length scales. *Proceedings of the National Academy of Sciences*, *108*(35), 14416–14421. <https://doi.org/10.1073/pnas.1107966108>